RSC Advances

ROYAL SOCIETY OF CHEMISTRY

www.rsc.org/advances

Table of Contents Entry

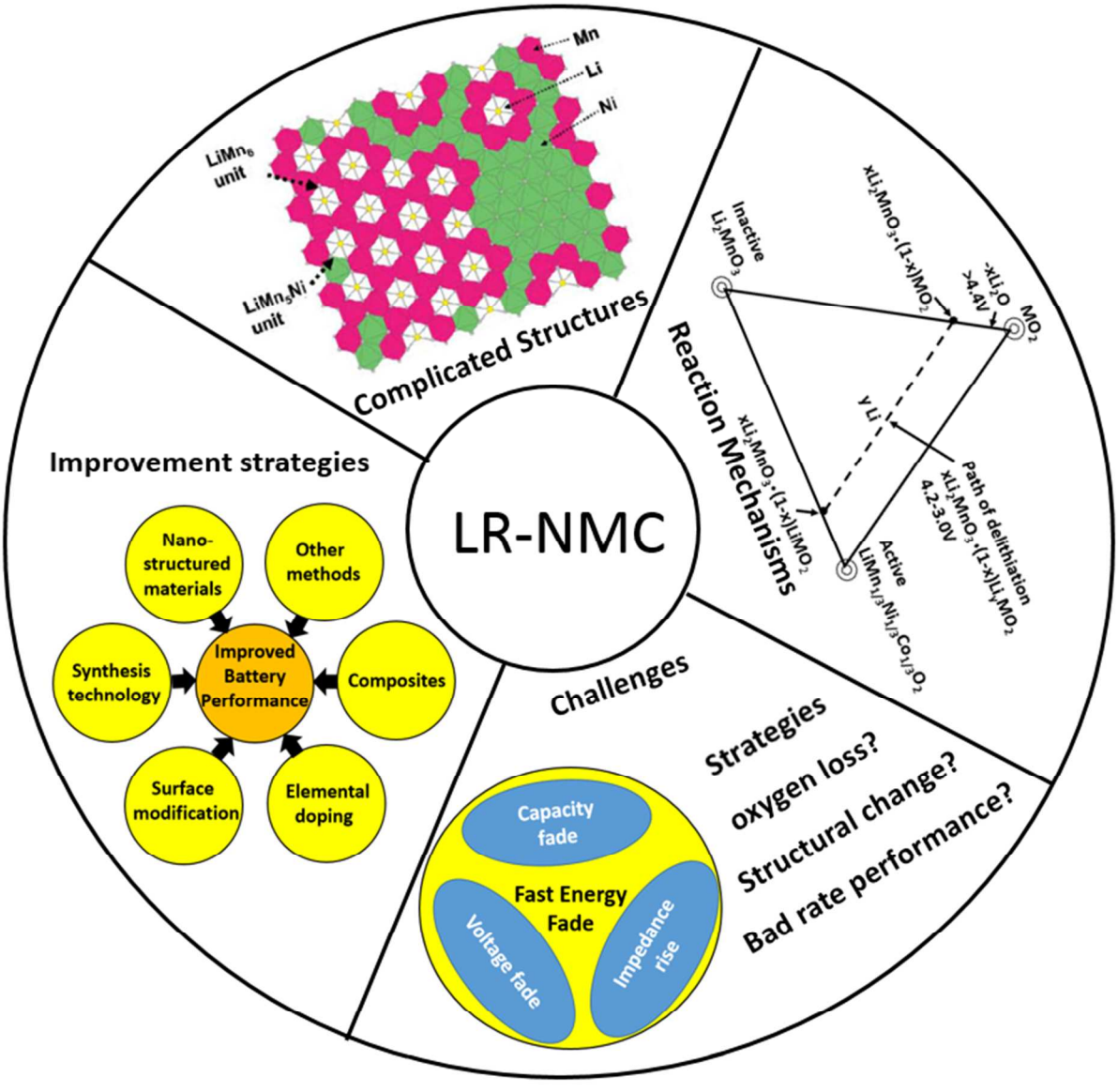

Importance of this review work:

This review systematically summarized Li-rich layered oxides and states the strategies to enhance such materials when used in Li-ion batteries.

Article

Recent Progress in Li-rich Layered Oxides as Cathode Materials for Li-ion Batteries

Jianhua Yan,[a,b] Xingbo Liu[b] and Bingyun Li [a,*]

Li-ion Battery represents one of the most important and most technically challenging components of electric vehicles. Cathode is one of the three key components (i.e., cathode, anode, and electrolyte) of Li-ion battery and determines the battery quality. The demand for higher energy density, lower cost, and environmentally friendly batteries make Li-rich layered oxides $xLi_2MnO_3 \cdot (1-x)LiMO_2$ (LR-NMC) one of the most attractive candidates for future cathode materials. In this review, we discussed the state-of-the-art research activities related to LR-NMC materials, including their structures, mechanisms of high capacity and large voltage, challenges, and strategies that have been studied to improve their performances. Finally, we concluded with some personal perspectives for the future development of LR-NMC materials.

[a]*Department of Orthopaedics, West Virginia University, Morgantown, West Virginia, USA 26506*
[b]*Department of Mechanical and Aerospace Engineering, West Virginia University, Morgantown, West Virginia, USA 26506*
**Correspondence to:*
Bingyun Li, PhD, Associate Professor
Director, Biomaterials, Bioengineering & Nanotechnology Laboratory
Department of Orthopaedics
West Virginia University, Morgantown, WV 26506-9196, USA
Tel: 1-304-293-1075, Fax: 1-304-293-7070, Email: bili@hsc.wvu.edu
URL: http://medicine.hsc.wvu.edu/ortho-bli/

Introduction

The heavy carbonaceous emissions from vehicle engines and shortages of fossil fuels have attracted increased research interest in electric vehicles including plug-in hybrid electric vehicles (PHEVs), hybrid electric vehicles (HEVs) and electric vehicles (EVs) [1]. Battery-powered electric vehicles use an electric motor for propulsion with batteries for electricity storage. The energy in the batteries provides motive and auxiliary power onboard the vehicle. Electric vehicles offer the prospect of low air pollutants and relatively low cost of the electric motor, as well as very high efficiency. The main drawback is their reliance on batteries that presently have very low energy and power densities compared to oil fuels. In fact, HEVs are the only type which have been largely sold on the market in the past years, and Ni-metal-hydride (NiMH) batteries dominate the HEV industry. However, the NiMH batteries have low specific energy (1-2 kWh) and high cost that have limited their use in PHEV or EV applications.

For PHEVs and EVs, Li-ion batteries (LIBs) seem to be promising [2] and great progress have been made in developing their cathode materials, which are a key component of LIBs and determine the quality of LIBs. Among the LIBs cathode materials studied, spinel oxides (LiM_2O_4), olivine phosphates ($LiMPO_4$), and layered oxides ($LiMO_2$) have attracted a significant amount of interest. $LiMn_2O_4$ is considered as a promising cathode material for LIBs due to its low cost, non-toxicity, and high thermal stability, and Ni-substitute $LiNi_{0.5}Mn_{1.5}O_4$ has been found to have high power density with an active potential of 5 V [3]. Olivine types of $LiFePO_4$ and $LiMnPO_4$ are of interest for use in large type LIBs due to their high intrinsic structural and chemical stability which have resulted in long cycle life batteries with low-cost and environmentally friendly properties [4]. The layered $LiMO_2$, in which M is a combination of Ni, Mn, and Co - so called NMC, is considered a potential next generation cathode material for LIBs since it has a moderate thermal stability and high rechargeable capacities (larger than 150 $mAhg^{-1}$) at high rates [5].

However, each kind of the above cathode materials have their limitations. The performance comparison for these materials is shown in **Table 1**. The battery system in the 40-mile PHEVs or EVs is expected to be designed with adequate cycle life and safety. Safety is a pre-requirement for power LIBs and LIBs with high energy density must be able to sustain high operating temperatures and poor working conditions. Most of all, the battery systems should have sufficient energy capacity and adequate output peak power, both of which are often considered as two key criteria during material optimization and development. The demands of electric drive vehicles (EDV) for power LIBs are shown in **Table 2** [6].

Table 1. Comparison of current commercialized cathode materials.

Performance	$LiCoO_2$	NMC	$LiMn_2O_4$	$LiFePO_4$
Cost/kwh	Higher	High	High	High
Safety	Poor	Poor	Average	Good
Cycle life	Average	Good	Average	Average
Power	Good	Good	Good	Average
Energy/whkg^{-1}	Good	Good	Average	Poor

Table 2. EDV demands for power LIBs.

EDV type	Weight (max. kg)	Peak Power (min. kw)	Power (min. wkg^{-1})	Capacity (min. kwh)	Energy (min. $whkg^{-1}$)
HEV	50	40-60	800-1200	1.5-3	30-60
PHEV	120	50-65	400-540	6-12	50-75
EV	250	50-100	200-400	25-40	100-160

In the near-term, the above cathode materials, and a few other types, will be optimised and used in PHEVs and EVs. In the longer-term, new battery chemistries with significantly higher energy densities need to be developed to enable the development and use of PHEVs and EVs with a longer all-electric range. The United States Department of Energy is currently supporting exploratory research on LR-NMC cathode materials because of their high reversible capacities (> 200 $mAhg^{-1}$) and high operating voltages (~ 4.8 V vs. Li/Li^+). Since the energy density of LIBs is determined by the material's reversible capacity and operating voltage, which are determined by the material intrinsic chemistry. Therefore, understanding their intrinsic chemistry is very important. In this regard, we will focus on the intrinsic chemistry of this family of materials in this review [7, 8].

In this review, we will highlight LR-NMC materials with complex structures and mechanisms in details, and will present their recent breakthroughs. Then, we will conclude with a summary of current and future research efforts and opportunities in the development of such cathode materials.

LR-NMC

A few years ago, Thackeray et al. [9] proposed a new sophisticated strategy to increase the stability and improve the electrochemical characteristics of lithiated Ni-Mn-Co-oxides. Structurally compatible units like Li_2MnO_3 were used as partial substituents in lithiated transition metal oxides. Li_2MnO_3 is considered the best stabilized component for the $Li[Mn_xNi_yCo_z]O_2$ electrode because it is electrochemically inactive over a wide potential window of 2.0-4.4 V and electrochemically active over 4.5 V [10-13]. With excess Li ions introduced, beyond the limitation of one Li ion per MO_2 formula, exceptionally high reversible capacities and energy densities (> 300 $mAhg^{-1}$ and 900 $WhKg^{-1}$) of these series of materials can be achieved when cycled between 2.0-4.8 V; besides, with the support of the stable structure of $LiMn_2O_3$, these materials have good capacity retention and thermal stability [14-17]. There is a high probability that such materials with a higher capacity utilization and lower running costs could be further developed. In this regard, LR-NMC has been proposed as one of the most promising candidates [18, 19]. In the following section, we will highlight the progress and challenges of LR-NMC cathode materials.

Structures

LR-NMC is represented by the general formula $xLi_2MnO_3 \cdot (1-x)LiMO_2$. Various design equations have been proposed to synthesize the materials, and high capacities can be obtained if x > 0.3 [20-23]. Park et al. [22] designed a phase diagram consisting of $LiNi_{1/2}Mn_{1/2}O_2$, $LiCoO_2$, and Li_2MnO_3, as shown in **Figure 1a**. The compositions located on the phase diagram can be expressed as $Li[Co_x(Li_{1/3}Mn_{2/3})_y(Ni_{1/2}Mn_{1/2})_{1-x-y}]O_2$. The Mn oxidation state of the solid solutions would be +4 in the triangular phase. The four samples shown in **Figure 1a** were characterized by X-ray diffraction (XRD), as shown in **Figure 1b**. All the patterns can be indexed to a single phase of the α-$NaFeO_2$ type with space group R3m. The splitting peaks of 104 and 018 were considered as evidence for the degree of ordering layered structures.

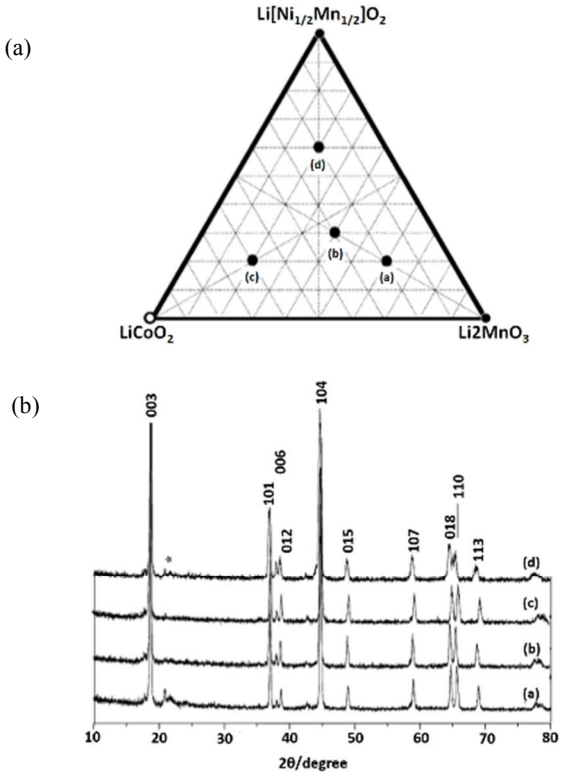

Fig. 1. (a) A new triangle phase diagram of $Li[Ni_{1/2}Mn_{1/2}]O_2$-$LiCoO_2$-Li_2MnO_3 system. (b) XRD patterns for samples (a)-(d) [22]. Reprinted with permission from © 2005 Elsevier B.V.

Structures made of these series of materials are hard to characterize and the reason for the complex structures may lie in the solid-solute phases formed by Li_2MnO_3 and $LiMO_2$; both Li and transition metal ions coexist in the transition metal layer. There has been a significant amount of work on understanding the highly complex structures [24-34]. First, Pan et al. [24] analyzed $Li[Li_{0.2}Cr_{0.4}Mn_{0.4}]O_2$ using X-ray absorption spectroscopy (XAS) and nuclear magnetic resonance (NMR), and provided evidence for the formation of Cr- or Mn-rich regions; in another word, there are different metal clusters in different areas. Then, by calculating the lattice parameters existing in the superstructures, Lu et al. [25] showed that the structural properties of these materials vary with compositions. They believed that a solid solution was formed with an ordering of Li ions and transition metal ions in the transition metal layer due to the differences in the oxidation states. Lei et al. [26] and Javis et al. [27] supported Lu et al.'s findings by examining $Li_{1.2}Ni_{0.2}Mn_{0.6}O_2$ with XRD, high resolution transmission electron microscope (HRTEM), scanning transmission electron microscope (STEM), energy dispersive X-ray spectroscopy (EDS), and electron energy loss spectroscope (EELS). $Li_{1.2}Ni_{0.2}Mn_{0.6}O_2$ was found to be composed of a solid solution with C2/m monoclinic symmetry and an ordering of Li-ions and transition metal ions in the transition metal layer due to differences in the oxidation states. Thackeray et al. [10] proposed a theory of "composite" mixture with Li_2MnO_3-like

and $LiMO_2$-like domains which was formed by structurally integrating Li_2MnO_3 into $LiMn_{0.5}Ni_{0.5}O_2$. As shown in **Figure 2a**, these "composite" structures have domains with short-range order, rather than true solid solutions in which the cations are uniformly distributed within discrete layers. The Li_2MnO_3 component was activated to form a MnO_2 component within a charged electrode structure, making these materials extremely versatile for tailoring and optimizing their composition, structure, and electrochemical properties. Yang et al. observed the two composites in $Li_{1.2}Ni_{0.15}Co_{0.1}Mn_{0.55}O_2$ by In situ XRD as shown in **Figure 2b** [32]. The disappearance of the (020) reflection peaks upon charging to the voltage plateau above 4.5 V is indicative of the disappearance of Li/Mn ordering within the Li_2MnO_3 component, which indicate that the $Li_{1.2}Ni_{0.15}Co_{0.1}Mn_{0.55}O_2$ material is a composite formed by conventional layered $LiMO_2$ (M = Ni, Co, Mn) and Li_2MnO_3 components. Yu et al. [61] illustrated the relationship between the electrochemical performance of this composite material and its composite components at room temperature. Kikkawa et al. [62] further supported this theory by observing two independent Fe- and Mn-rich nanodomains in $Li_{1.2}Mn_{0.4}Fe_{0.4}O_2$ with STEM and EELS. They found that Li ions were first depleted from Fe-rich nanodomains and subsequently extracted from the whole region.

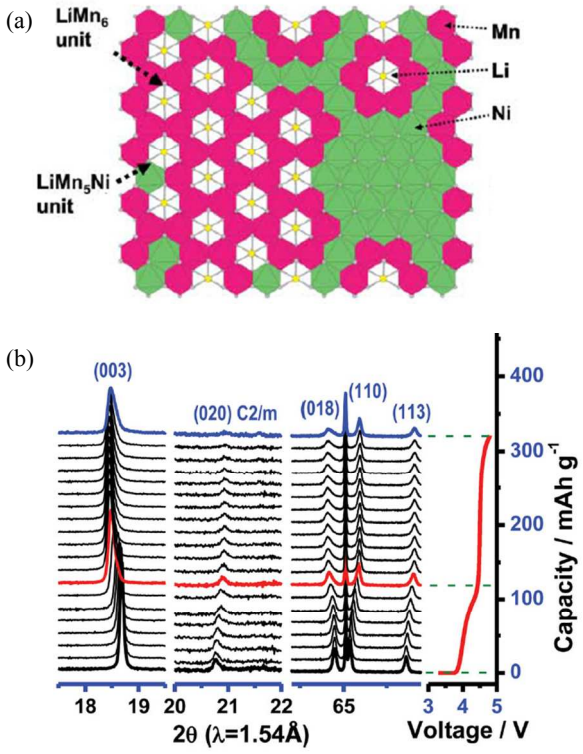

Fig. 2. (a) Schematic structural illustrations corresponding to $Li_{1+x}(Mn_{0.5}Ni_{0.5})_{1-x}O_2$ [10] and (b) In situ XRD patterns collected during the first charge for $Li_{1.2}Ni_{0.15}Co_{0.1}Mn_{0.55}O_2$ material [32]. Reprinted with permission from © 2011 American Chemical Society [10] and © 2013 WILEY-VCH Verlag GmbH & Co. KGaA, Weinheim [32].

Until now, there are no definitive conclusions about the complex structures for this family of materials. However, the integrated composite theory seems to be well accepted. Due to the isostructural of Li_2MnO_3 and $LiMO_2$, the composite forms and layers of Li^+ ions alternate with layers containing a mixture of Li^+, Mn^{4+}, and M^{3+} ions in a cubic close-packed oxygen array. The presence of both Li^+ and Mn^{4+} in the transition metal layer reduces the symmetry of Li_2MnO_3 from the R3m group to C2/m. Composites of two layered components of Li_2MnO_3 and $LiMO_2$ are particularly attractive for designing electrodes in which Li is cycled in and out of the layered $LiMO_2$ component while using the structurally compatible and, from a capacity standpoint, electrochemically inert Li_2MnO_3 component to provide stability to the electrode at a high voltage [28, 33].

Mechanisms of high voltage and large capacity

The capacity of LR-NMC family of materials is commonly larger than 200 $mAhg^{-1}$ with a high voltage plateau of ~ 4.8 V. Many studies have been initiated in an attempt to determine the underlying mechanism(s) for the high capacity delivered by these materials [31, 35-41]. Two distinct regions are exhibited during the first charge as shown in **Figure 3** [38]. The initial sloping region A corresponds to the oxidation of the transition metal ions to M^{4+}. In this stage, Li_2MnO_3 cannot be oxidized because of the high oxidation state of Mn^{4+}. The following plateau region B, ~ 4.5 V, corresponds to a quick capacity increase due to the extraction of Li^+ from Li_2MnO_3 [39, 40], which in turn leads to the formation of the MnO_2 host structure in the compound which can then reversibly intercalate Li-ions. However, the initial discharge profile presents a large irreversible capacity. After the first cycle, this material still have a high capacity and capacity retention. Some researchers [19,34, 35, 741] believed that a transformation from a layered structure to a spinel-like and layered mixed structure takes place after a deep delithiation-lithiation during the initial charge, and this transformation leads to the initial capacity fade. The transformed spinel-like nanodomain structure may offer excellent capacity retention as well as good rate capability in the subsequent long-term cycles. Additionally, other researchers found the initial capacity fade was also associated with Ni dissolution accompanied by an increase in oxidation states of remaining transition metals at surface regions of particles [28].

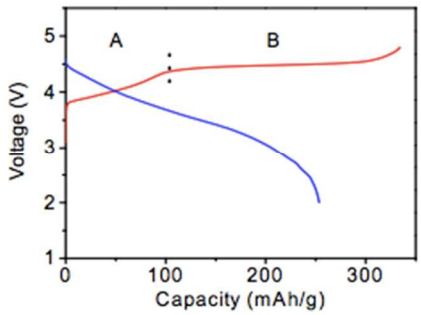

Fig. 3. Schematic charge-discharge profiles of $xLi_2MnO_3 \cdot (1-x)\ LiMO_2$ [38]. Reprinted with permission from © 2007 Journal of Electrochemical Society.

In general, two major mechanisms concerning the initial charge-discharge processes have been discussed. The first theory is the oxygen ejection mechanism proposed by Lu and his colleagues [19]. They found that the capacity loss corresponded to the simultaneous

removal of Li and O from the structure at the 4.5 V plateau. After the plateau, the cell could deliver stable reversible capacity between 2.0 and 4.6 V. Oxygen evolution was observed during the first charge process by in situ electrochemical mass spectroscopy measurements by Armstrong et al. [42]. The irreversible capacity loss was due to the extraction of Li as ''Li_2O" on charging beyond the oxidation of the transition metal ions above the 4^+ state and the inability to insert all the Li-ions back into the lattice during discharge. The elimination of oxide ion vacancies at the end of the first charge led to a decrease in the number of Li-ion sites, resulting in a difference between the first charge and discharge capacity values. Additionally, after the initial charge, the transition metal moved into the Li layer to form a skeleton structure. Koyama et al. [39] and Xiao et al. [43] further supported this theory by calculating the oxygen stability with density functional theory (DFT+U) electronic structure calculations. Recently, Arunkumar and Wu [44] identified factors that control the amount of oxygen loss and capacity fading. The amount of oxygen loss, which in turn influences the reversible capacity values in subsequent cycles, was determined by the amount of Li in the transition metal layer of the solid solution before charge. The tendency of Ni^{3+} to be reduced to Ni^{2+} and the consequent volatilization of Li during synthesis altered the Li content in the transition metal layer thereby influencing the degree of oxygen loss and reversible capacity values. A high Mn^{4+} content contributed to a decrease in oxygen mobility and loss during the initial charge.

A second major theory is the H^+ exchange mechanism proposed by Robertson and Bruce [45]. According to their work, the electrochemical activity of Li_2MnO_3 was found to involve the exchange of Li^+ by H^+ that leads to the formation of $Li_{0.62}H_{1.29}MnO_{2.95}$. At discharge, $Li_{0.62}H_{1.29}MnO_{2.95}$ goes back to $Li_{1.28}H_{0.66}MnO_{2.97}$. Armstrong et al. [46] supported this mechanism, and found a lot of H generation whose content corresponded to the amount of extracted Li^+ ions at the plateau of above 4.5 V. In addition, Johnson et al. [47] and Li et al. [48] found that some electrodes might deliver initial discharge capacities that exceed their theoretical values, and proton exchange might have contributed to such an anomalous phenomenon.

In fact, both mechanisms may occur after electrochemical activation to 4.6 or 4.8 V. A typical schematic compositional phase diagram showing the electrochemical reaction pathways for $xLi_2MnO_3 \cdot (1\text{-}x)LiMO_2$ is shown in **Figure 4a** [49]. The initial charge process on a Li_2MnO_3-$LiMO_2$-MO_2 phase diagram of $0.3Li_2MnO_3$-$0.7LiMn_{1/3}Ni_{1/3}Co_{1/3}O_2$ was used as the composition of a parent reference electrode. Li was initially extracted from the $LiMO_2$ component of the electrode structure, typically at potentials < 4.4 V vs. Li^0, with concomitant oxidation of the transition metal ions to M^{4+}. Thereafter, Li was extracted from the Li_2MnO_3 component (> 4.4 V) accompanying irreversible loss of oxygen from the lattice as confirmed by in-situ XRD [25] and differential electrochemical mass spectrometry studies [42] or from the proton exchange. At the same time, activation of the transition metal ions, such as Ni^{2+}/Ni^{4+} and Co^{3+}/Co^{4+}, also increased and resulted in a high capacity [9, 50, 51]. The Li extraction accompanying the oxygen loss facilitated the lowering of the oxidation states of the transition metal ions at the end of the first discharge thereby leading to a high reversible capacity in the subsequent charge-discharge cycles. If all the Li was to be removed from the electrode, Johnson et al. [9, 47] described that the two-step process during charge could be expressed by the following reactions:

$$xLi_2MnO_3 \cdot (1\text{-}x)LiMO_2 \rightarrow xLi_2MnO_3 \cdot (1\text{-}x)MO_2 + (1\text{-}x)Li \quad (1)$$

$$xLi_2MnO_3 \cdot (1\text{-}x)LiMO_2 \rightarrow xMnO_2 \cdot (1\text{-}x)MO_2 + xLi_2O \quad (2)$$

In addition to the Mn redox reactions, the charge compensation of oxygen may also contribute to high capacity. When increasing the potential in excess of 4.8 V, the charge-discharge cycling properties decreases. It is believed that changes in material structures have occurred due to the charge compensation of oxygen [9]. Since it was effective to embed inactive Li_2MnO_3 component within a $LiMO_2$ structure to stabilize electrodes at high potentials, there are two strategies to generate high-energy batteries with the conventional layered cathode materials. They are changes that occur to the compositional, structural, and electrochemical properties of the electrodes and the importance of using a relatively high Mn content and a high charging potential (> 4.4 V) to generate high capacity electrodes [10, 47].

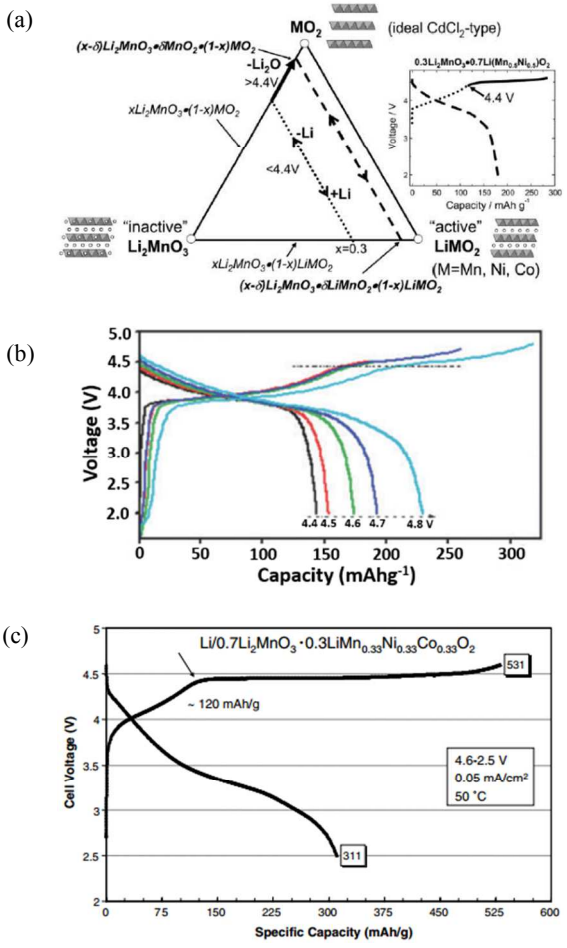

Fig. 4. Electrochemical performance of xLi_2MnO_3-$(1\text{-}x)LiMn_{1/3}Ni_{1/3}Co_{1/3}O_2$. (a) Li_2MnO_3-$LiMO_2$-MO_2 compositional phase diagram; (b) the charge-discharge curves for the 1st cycle of $0.3Li_2MnO_3$-$0.7LiMn_{1/3}Ni_{1/3}Co_{1/3}O_2$; (c) initial charge-discharge profiles at 50 °C of a $Li/0.7Li_2MnO_3$-$0.3LiMn_{0.33}Ni_{0.33}Co_{0.33}O_2$ cell (0.05 mA/cm^2) [47, 49, 50]. Reprinted with permission from © 2007 [49] and 2012 [50], Royal Society of Chemistry. Reprinted with permission from © 2007 Elsevier Ltd [47].

The profiles of the initial charge-discharge cycles of a Li/0.3Li_2MnO_3-0.7$LiMn_{1/3}Ni_{1/3}Co_{1/3}O_2$ cell are presented in **Figure 4b** [50]. During the initial charge of the cell to approximately 4.4 V, Li was extracted from the $LiMO_2$ component with a concomitant oxidation of the Ni and Co ions, while the Mn ions remained tetravalent until the Li_2MnO_3-MO_2 tie-line was reached. During this reaction, depletion of Li ions from the Li layer was compensated by the diffusion of Li from octahedral sites in the Mn layer of the Li_2MnO_3 component to tetrahedral sites in the Li-depleted layer thereby providing the additional binding energy necessary to maintain structural stability. Therefore, the Li_2MnO_3 component acted as a reservoir of surplus Li that could be used to stabilize the electrode structure at low Li loadings. If the electrochemical potential of the cell was raised above 4.4-4.8 V during charge, Li could be further extracted from the electrode as indicated by the solid line in the compositional phase diagram, and the capacity increased from 145 $mAhg^{-1}$ to 235 $mAhg^{-1}$. The initial charge capacity was therefore related to the voltage applied. Continuing increasing the voltage may further increase the initial discharge capacity. As shown in **Figure 4c** [47], an anomalous discharge capacity of 311 $mAhg^{-1}$, exceeding the theoretical values [242 $mAhg^{-1}$, calculated from reactions (1) and (2)] for lithiation back to the rocksalt stoichiometry, has been observed for 0.7Li_2MnO_3-0.3$LiMn_{0.33}Ni_{0.33}Co_{0.33}O_2$. A possible explanation for the higher-than-expected capacity was possible side reactions involving electrolyte oxidation and proton exchange [47, 51].

Challenges

LR-NMC can provide high capacity and seem to be an attractive candidate for LIBs applications. However, LR-NMC has two well-known limitations: a large irreversible initial capacity loss (40-100 $mAhg^{-1}$) and poor rate performance. The irreversible capacity loss is associated with the elimination of oxide ion vacancies from the layered lattice at the end of the first charge, which will quickly react with carbonate-based solvent thus generating inactive by-products at high operating voltages (e.g., 4.8 V). The poor rate performance is associated with the insulating Li_2MnO_3 component and the thick solid/electrolyte interfacial (SEI) layer formed by a reaction of the cathode surface with electrolytes.

A third concern with LR-NMC is its fast energy fade with cycling. There are three major contributors to energy fade: (i) impedance rise which may be because Li atoms occupy different oxide sites during charge and discharge for the same voltage and/or capacity. The pulse discharge/charge behavior, characterized by an empirical parameter called the area specific impedance (ASI), is influenced by electrode thickness. It serves as a quick and simple means to estimate the impedance of cell under given conditions. (ii) Voltage fade and hysteresis which arises from crystal structural transformation in the oxide. (iii) Capacity fade because of the difficulty for Li^+ trapping in negative SEI film that caused by the crystal structural changes during cycling. Among these three factors, voltage and capacity fade contributes ~ 90% to the energy fade and this implies that there are still rooms for improvement with electrode/electrolyte optimization [52].

The voltage fade and capacity fade are associated with internal phase transitions. Some preliminary results [53-55] indicated that voltage fade was unaffected by coatings, additives, cation doping, and substitution. Whereas, the cut-off voltage and cation ordering in the crystal structure substantially influenced voltage fade. First, the lower the cycling cut-off voltage the less voltage fades. No voltage fades occur when upper cut-off voltage of 4.3V is used as cycling voltage. Secondly, improving Li mobility at top of charge and controlling cation disorder for all states of charge could mitigate voltage fade. In addition, Croy et al. [56] presented that the voltage fade and hysteresis were both increasing with increasing Li_2MnO_3 content. However, the structural change during cycling was not clearly understood. On the other hand, although the initial cycle treatment is useful for capacity retention, the "activation" leads to irreversible structural changes, surface damage, voltage fade, and hysteresis. Voltage fade and capacity fade are critical for energy fade, thus the structural change and corresponding mechanisms must be further studied. For example, what are the possible structural changes of the electrode materials during the initial charge-discharge processes of the Li-extraction and upon prolonged cycling? How do the electrodes' performances correlate with structure, morphology, and thermal behavior of LR-NMC materials? In addition, the reaction mechanism, which may lead to structural changes, is also not clearly understood. Questions remain related to the abnormal phenomenon of excess capacity beyond the theoretical values [57, 58] and where oxygen goes during the initial charge and discharge. Although the two well-known mechanisms have been proposed and discussed above, there are still many concerns. For instance, in the oxygen evolution mechanism, where does the oxygen go after its removal from the cathode structure? If it goes to the electrolyte, it could threaten the safety of the battery. Hong et al. [37] even argued that there was not any oxygen ejection from the structure and the oxygen formed a π bonding with transition metal at the 4.5 V plateau. In the H^+ exchange mechanism, the H^+ is generated in the electrolyte, but does this influence the stability of the cathode structures? Assuming both of these mechanisms about the initial cycle are correct, how about subsequent cycles? There is very little literature addressing these issues.

In addition, it is difficult to find the other battery components (i.e., anode and electrolyte) that can match the wide-range of voltage of LR-NMC class of materials to assemble a battery. To achieve a high capacity, generally the charge-discharge potentials applied to the cells are between 2.0 and 4.8 V. Different discharge cut-off potentials give different capacities as shown in **Figure 4b**. To achieve optimal performance, the batteries generally operate below a specific working potential, above which the electrochemical performance suffers. Therefore, chemists must find suitable anode materials and novel electrolytes; electrolyte erosion at high voltage is a major concern. Also, chemists must control side effects such as poor cycle life, safety issues, and poor rate capability with the increasing voltage plateau. Recently, for example, Envia-System reported a layered-layered $Li_2MnO_3 \cdot LiMO_2$ composite based battery with high energy density of 400 $WhKg^{-1}$. This battery used nano Si-C composite as an anode material and a high-voltage new electrolyte with additives. However, there are some limitations. The high irreversible capacity loss is undesirable, oxygen loss leads to gassing

in pouch cells, and fade in average voltage upon cycling and high Mn dissolution lead to poor cycle life and calendar life [7].

Improvement strategies

To overcome the performance degradation and to decrease cost of LR-NMC materials, efforts, such as optimizing synthesis method, surface modification, elemental doping, use of composites and nanosized materials, and others, have been investigated.

Synthesis technology. While the search for high performance LR-NMC for LIBs remains a primary objective, cost associated with producing these materials is now becoming another overriding factor. Sustainability, renewability, and green chemistry concepts must be taken into consideration when selecting cathode materials and processing methods for LR-NMC based batteries, especially for high volume applications. Synthesizing technology has a great impact on atomic order and subsequently affects the crystallinity degree, micro morphology, and distribution of material components. The electrochemical properties were also found to depend on the cooling rate used during material synthesis [59, 60]. Thus, selecting suitable processing methods is of importance.

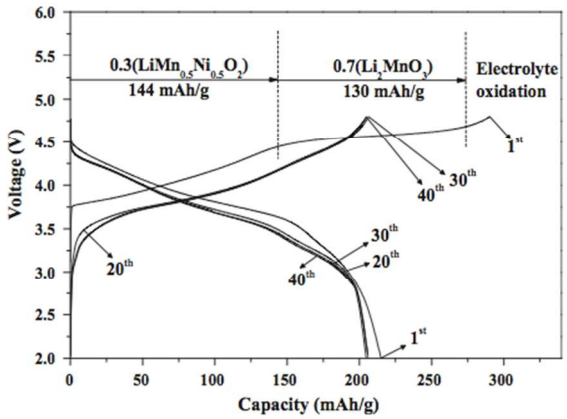

Fig. 5. Cycling properties of the cathode powders with post-treated at 800 °C [64]. Reprinted with permission from © 2012 Elsevier Ltd.

The common processing methods for LR-NMC include coprecipitation [61, 62], spray pyrolysis [63, 64], simple solid-phase [65], combustion [66], molten salt [67], sol-gel [68, 69], hydrothermal [70, 71], ball-milling-annealing [72], carbon-thermal reduction [73], and others [74-76]. Generally speaking, the hydrothermal process has the lowest cost and it can be easily tuned to obtain nanostructures using different solvents, co-solvents, or surfactants. The co-precipitation process depends on the precipitation and crystallization of the targeted compounds under normal temperature and pressure conditions. The secondary particles prepared by this method are spherical with uniform sizes, which ensure a more stable performance. For example, Li et al. [62] synthesized a high-voltage layered $Li[Li_{0.2}Mn_{0.56}Ni_{0.16}Co_{0.08}]O_2$ cathode material by the co-precipitation method. After the initial decay, no obvious capacity fading was observed when cycling the material at different rates. Steady-state reversible capacities of 220 $mAhg^{-1}$ at 0.2 C, 190 $mAhg^{-1}$ at 1 C, 155 $mAhg^{-1}$ at 5 C, and 110 $mAhg^{-1}$ at 20 C were achieved in long-term cycle tests within the voltage cut-off limits of 2.5 and 4.8 V at 20 C. The spray pyrolysis is a versatile process with regard to the powder synthesis of inorganic and metal materials. The advantages of spray pyrolysis are that control of particle size, particle size distribution, and morphology are possible. The electrochemical performance of $0.3Li_2MnO_3$-$0.7LiNi_{0.5}Mn_{0.5}O_2$ cycled between 2.0-4.8 V at room temperature and 30 mAg^{-1} is shown in **Figure 5** [64]. The initial charge capacity of the cell was 290 $mAhg^{-1}$, in which 144 $mAhg^{-1}$ was delivered by $LiNi_{0.5}Mn_{0.5}O_2$ and 130 $mAhg^{-1}$ by Li_2MnO_3. The high first-cycle irreversible capacity loss of the cell was typical of a double-layered composite electrode. However, in subsequent cycles, the coulombic efficiency remained at nearly 100% and the discharge capacity of the cell decreased from 215 $mAhg^{-1}$ to 205 $mAhg^{-1}$ by the 40th cycle with capacity retention of 95%.

Surface modification. Surface modification is an important method to improve the electrochemical performance by means of providing a protection layer to minimize the direct contact of the active material with electrolyte or modifying surface chemistry [77]. LR-NMC materials have certain problems such as first-cycle irreversible capacity loss and inferior rate capability. What's more, structural and compositional stability under electrochemical cycling limits the useful capacity of the oxides for practical applications, because material degradation could result in declining performance and safety concerns. Any side reactions that consume or produce Li-ions change the capacity balance between anode and cathode. Such changes are irreversible and can be accumulated throughout the cycling processes, and may eventually lead to a significant capacity fade [78, 79]. Optimizing the surface region of layered oxide grains is of particular importance since the surface not only experiences Li insertion/extraction as the bulk, but also serves as the interface between cathode and electrolyte.

Surface coating has proven to be effective in improving capacity retention, rate capability, and even thermal stability of LR-NMC materials. The main mechanisms for the positive effect of surface coatings on the performance of this family of materials include: (1) forming a physical protection barrier that reduces possible side reactions between cathode and electrolyte. The surface coatings may stabilize the surface and interface of the cathode active materials, decrease oxygen loss, and suppress phase transition. (2) Acting as a hydrogen fluoride (HF) scavenger to reduce the acidity of non-aqueous electrolyte and suppress Mn^{3+} dissolution from cathode. (3) Modifying cathode surface chemistry to improve rate capability [78].

One possible way to extend cathode life and enhance rate capability of LR-NMC materials is to coat particle surfaces with carbon or metal oxides. A variety of materials such as C [80], ZrO_2 [81], TiO_2 [82], Al_2O_3 [81, 83], MgO [84, 85], and Ni and Mn composite oxides [86] have been used for surface coating and shown improved performances. For example, Zhao et al. [85] prepared MnO-coated $Li[Li_{0.2}Ni_{0.2}Mn_{0.6}]O_2$ and obtained high reversible capacities of 211 and 210 $mAhg^{-1}$ at high discharge rates of 1 C and 2 C, respectively, after 50 cycles. Myung et al. [81] reported that Al_2O_3-coated $Li[Li_{0.05}Ni_{0.4}Co_{0.15}Mn_{0.4}]O_2$ had good cyclic performances with a discharge capacity of 175 $mAhg^{-1}$ under 30 mAg^{-1}. In these materials, the coated metal oxide layer was transformed into a metal fluoride layer during cycling, as proved by secondary ion mass

spectroscopy. The newly formed metal fluoride layer was quite effective against HF attack during cycling. AlF_3 [87-90] was also widely studied as a coating layer due to its effectiveness against HF attack during cycling and high active energy to destroy Al-F bonds. **Figure 6a** [88] shows the initial charge and discharge curves of the uncoated and AlF_3-coated $Li(Li_{0.17}Ni_{0.25}Mn_{0.58})O_2$ with a cut-off potential of 2.0-4.8 V. The initial charge capacities of the uncoated and AlF_3-coated samples had the same value of 275 $mAhg^{-1}$, while the discharge capacities were 210 and 246 $mAhg^{-1}$, respectively. The Coulombic efficiencies for the initial charge and discharge capacities of the uncoated and AlF_3-coated samples were 76.4% and 89.5%, respectively. The polarization in the high potential region was lower for the AlF_3-coated sample (inset in **Figure 6a**), resulting in the effective Li extraction and subsequent Li insertion. Apparently, the decomposition of electrolytes at the end of the initial charge was greatly suppressed in the AlF_3-coated samples. **Figure 6b** compares the discharge capacities of the uncoated and AlF_3-coated samples. Clearly, the AlF_3-coated sample delivered a discharge capacity about 20% higher than the uncoated one. After 49 cycles, the discharge capacity of 232 $mAhg^{-1}$ still remained for the AlF_3-coated samples, indicating that the cyclic stability can be improved by AlF_3 surface coatings.

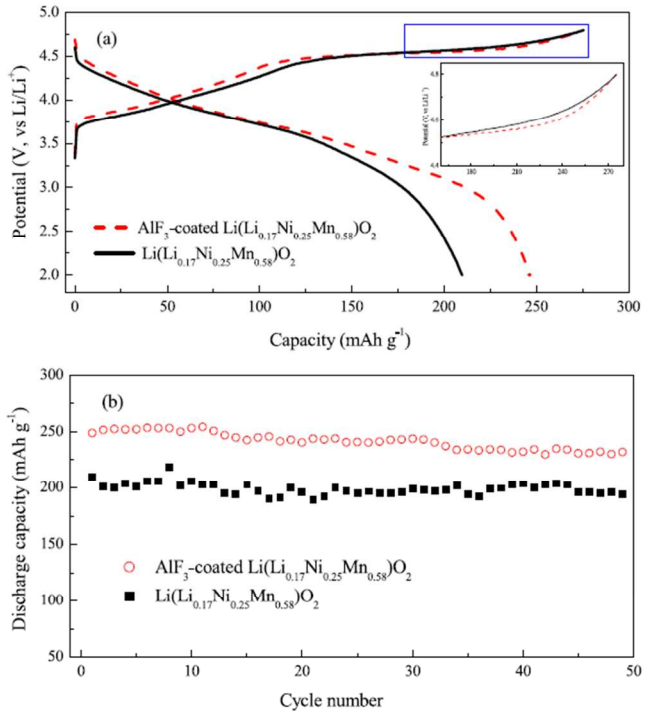

Fig. 6. (a) The first charge-discharge curves and (b) cycle performance of the as-prepared and AlF_3-coated $Li(Li_{0.17}Ni_{0.25}Mn_{0.58})O_2$ at 0.2 C rate [88]. Reprinted with permission from © 2012 Elsevier Ltd.

Besides carbon and metal oxides and fluorides, a variety of hydroxides and inert phosphates with host structures for Li^+ insertion/de-insertion such as $AlPO_4$ and $Co_3(PO_4)_2$ [91, 92], $LiCoPO_4$ [93], $LiNiPO_4$ [94], $LiMnPO_4$ [95], and Al(OH) [96] have been used as coating materials and shown to be effective in improving initial capacity retention and rate capability. For example, Kang and Thackeray [94] coated $0.5Li_2MnO_3{\cdot}0.5LiNi_{0.44}Co_{0.25}Mn_{0.31}O_2$ with $LiNiPO_4$ and achieved an initial discharge capacity of 200 $mAhg^{-1}$ under 1 C in comparison with ~170 $mAhg^{-1}$ without coating. Wang et al. [92] fabricated double-coated layers: an inner layer of 2 wt.% $AlPO_4$ or 2 wt.% $CoPO_4$ and an outer layer of 2-3.5 wt.% Al_2O_3 on $Li[Li_{0.2}Mn_{0.54}Ni_{0.13}Co_{0.13}]O_2$. The capacity of their modified material was above 215 $mAhg^{-1}$ at 2 C and, at low discharge rate, was up to 295 $mAhg^{-1}$ with only 26 $mAhg^{-1}$ capacity loss.

In addition to surface coating, changing surface chemistry is another effective way to improve structural and thermal stability therefore performance of LR-NMC materials. For instance, some transition metal ions can enter the lattice matrix of cathode materials during annealing and stabilize the cathode structure. As a result, electrode resistance, side reactions, and heat generation during cycling can be reduced, and improved cycle life, rate capability, reversible capacity, coulomb efficiency, and overcharge tolerance can be obtained [77, 97]. Kim et al. [98] reported that HNO_3-treatment of $0.3Li_2MnO_3{\cdot}0.7LiMn_{0.5}Ni_{0.5}O_2$ electrodes significantly improved the coulombic efficiency of the initial charge-discharge reaction but unfortunately decreased the initial discharge capacity from 259 to 205 $mAhg^{-1}$. Denis et al. [99] treated $Li[Li_{0.2}Mn_{0.54}Ni_{0.13}Co_{0.13}]O_2$ cathode with $(NH_4)_2SO_4$ solution and achieved a capacity of 230 $mAhg^{-1}$ at 1.2 C discharge rate. The high capacity was attributed to the surface transformation from a layered structure into a spinel structure along with part of the Li ions de-insertion [34, 41]. Materials with spinel structures have three-dimensional diffusion channels for Li-ions which may lead to good rate performances. Abouimrane et al. [100] treated $Li_{1.12}Mn_{0.55}Ni_{0.145}Co_{0.1}O_2$ using a thermal reduction method, and obtained capacities of 231 and 196 $mAhg^{-1}$, respectively, under 0.8 C and 1.6 C discharge rates. Zhang et al. [101] prepared surface nitrided $Li[Li_{0.17}Ni_{0.25}Mn_{0.58}]O_2$ cathode. The discharge capacity, high-rate capability, and cyclic stability of the nitrided samples improved dramatically in comparison with the untreated samples (**Figure 7**). The high-rate discharge capabilities of the nitrided and untreated samples were investigated at different rates (0.1, 0.2, 0.5, 1, 3 and 5 C with 1 C = 300 mAg^{-1}), as illustrated in **Figures 7a** and **7b**. The discharge capacities of the untreated sample were 126.7 $mAhg^{-1}$ at 5 C, while for the nitrided sample, the discharge capacity at the 5 C rate was 164.7 $mAhg^{-1}$. The improved high-rate capability of the nitrided sample was probably due to fast charge-transfer kinetics arising from the surface nitridation treatment. The cyclic properties for the nitride and untreated samples were shown in **Figures 7c** and **7d**. At a low current density of 0.1 C, the cyclic stability of the nitride sample was improved and after 60 cycles, the discharge capacity of the nitrided samples was 256 $mAhg^{-1}$, demonstrating a good capacity retention. By contrast, the discharge capacity of the untreated samples quickly decreased from 224 $mAhg^{-1}$ to 141 $mAhg^{-1}$ after 57 cycles. At a higher discharge rate of 1 C, the nitrided samples still showed better performances than the untreated samples. Zheng et al. [102] reported the effects of persulfate treatment on $Li[Li_{0.2}Mn_{0.54}Ni_{0.13}Co_{0.13}]O_2$, and found that $Na_2S_2O_8$ treatment greatly improved the first cycle efficiency of the active material to nearly 100%, and the rate performance was also increased to > 200 $mAhg^{-1}$ at 1 C rate. The reason for the improved rate performance following $Na_2S_2O_8$ treatment was probably attributed to the formation of the spinel phase on material surface

and the extraction of Li and oxygen, which may result in decreased electrochemical resistance.

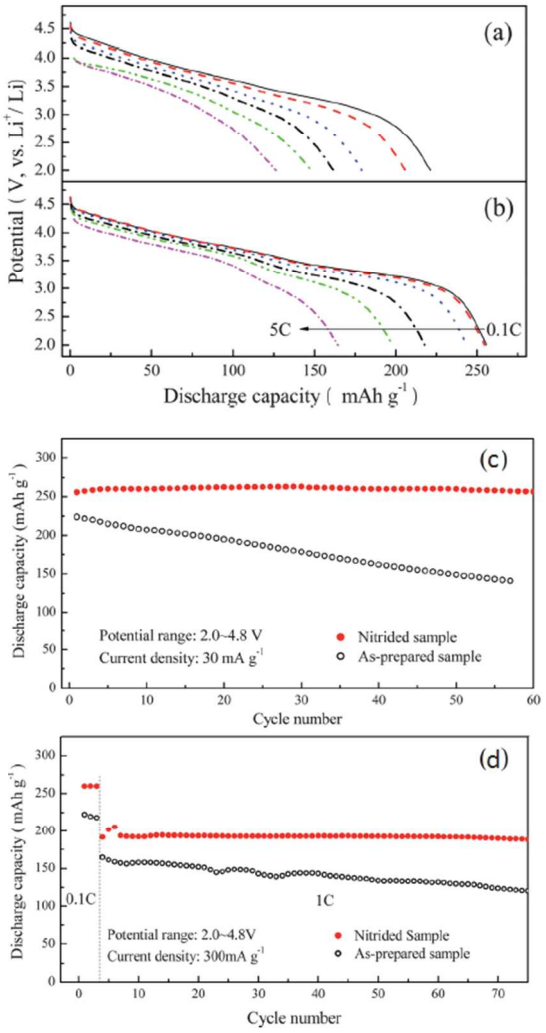

Fig. 7. Rate capabilities of the (a) as-prepared and (b) nitrided $Li[Li_{0.17}Ni_{0.25}Mn_{0.58}]O_2$ at 0.1, 0.2, 0.5, 1, 3 and 5 C rates (1 C = 300 mAg^{-1}). Cycle performances of the (c) as-prepared and (d) nitrided $Li[Li_{0.17}Ni_{0.25}Mn_{0.58}]O_2$ electrodes [101]. Reprinted with permission from © 2012, Royal Society of Chemistry.

In summary, surface modifications seem to be effective in improving the performance of LR-NMC materials. However, there are still some concerns. For instance, AlF_3 is an insulator to both electrons and Li ions, and a thicker coating would lower the kinetics of the charge-transfer reaction at the coating/active material interface. Therefore careful control of layer thickness must be achieved for such coatings. Also, how to combine excellent electronic conductivity with inert physical protection from the same coating layer still needs more investigation. In addition, to achieve uniform coatings could be challenging [77, 78, 103], and the correlation between surface chemistry and material performance has not been systematically investigated.

Elemental doping. As previously discussed, the poor rate capability of LR-NMC materials is related to the inferior electronic conductivity in conjunction with Mn^{4+} ions [10]. Moreover, part of the Li_2MnO_3 component is likely to transform from a layered structure to a spinel-like region at the end of the first discharge process and the amount of transformed component may increase upon further extraction/reinsertion of Li [77, 97]. An elemental doping strategy is considered to assist in those transferred spinel-like regions to enhance electron and ion flows in local phases. The performance, including rate and cyclic capability, can be improved by elemental doping, through either affecting the microstructure or morphology or stabilizing the layered crystal structures.

In general, the elemental doping technology includes cation doping and anion doping. Cation doping like doping Ti [73], Co [104, 105], Al [71, 106, 107], Fe [71, 73], Ru [108], Cr [63, 109], or Mg [110, 111] can improve conductivity, enlarge lattice constants, and form a stronger M-O bond (M=Ti, Co, etc.), all of which are favorable for the migration of Li ions and maintainance of a stable crystal structure [112]. Tang et al. [104] compared the electrochemical performances of $Li[Li_xMn_{0.65(1-x)}Ni_{0.35(1-x)}]O_2$ with and without Co doping. Results showed that the Co-doped $Li[Li_{0.0909}Mn_{0.588}Ni_{0.3166}Co_{0.0045}]O_2$ had a higher initial efficiency of 78.8% and a higher energy density of 858.4 $Whkg^{-1}$ compared to 56.5% and 590.1 $Whkg^{-1}$ for the un-doped ones. Kim et al. [105] found a Co doped Li-rich layered cathode had a lower impedance value during cycling with improved capacity and rate capability comparing to an un-doped one. It is considered that the higher capacity and superior rate capability of the Co-doped samples, especially for the $Li[Li_{0.1}Ni_{0.3}Co_{0.1}Mn_{0.5}]O_2$, were associated with reduced resistance of the electrode during cycling. Jiao et al. [99] prepared $Li[Li_{0.2}Ni_{0.2-x/2}Mn_{0.6-x/2}Cr_x]O_2$ (x = 0, 0.02, 0.04, 0.06, 0.08) by doping Cr using a sol-gel method. Doping Cr could reduce the electrochemical impedance of such materials and improve their capacities and rate capabilities; the best electrochemical property was achieved when the amount of Cr was 0.04. Similarly, Park et al. [107] reported that doping Al could reduce the electrochemical impedance and improve performances. Song et al. [108] reported significant improvements in $0.55Li_2MnO_3 \cdot 0.45LiNi_{1/3}Co_{1/3}Mn_{1/3}O_2$ cathode by doping Ru. The initial discharge capacity and cyclic capability at a high discharge current density of 1 C or 2 C varied substantially between the Ru-doped and non-Ru-doped cathodes, although there was not a big difference in the performances for the Ru-doped and non-Ru-doped cathodes at a low current of 0.05 C or 0.2 C as shown in **Figures 8a** and **8b**. In addition, from **Figure 8c**, the average columbic efficiency of the Ru-doped cathode was 99.7% and the capacity fade was as small as 0.06% per cycle in comparison with 0.13% per cycle for the un-doped; these findings implied good capacity retention at a high charge-discharge rate. The significant improvements could be due to the increase in Li inter-slab distance upon Ru doping, which lowers the activation barrier for Li diffusion in both compounds of $LiNi_{1/3}Co_{1/3}Mn_{1/3}O_2$ and $LiMn_2O_3$ and hence forms more Li reinsertion/extraction in the structures.

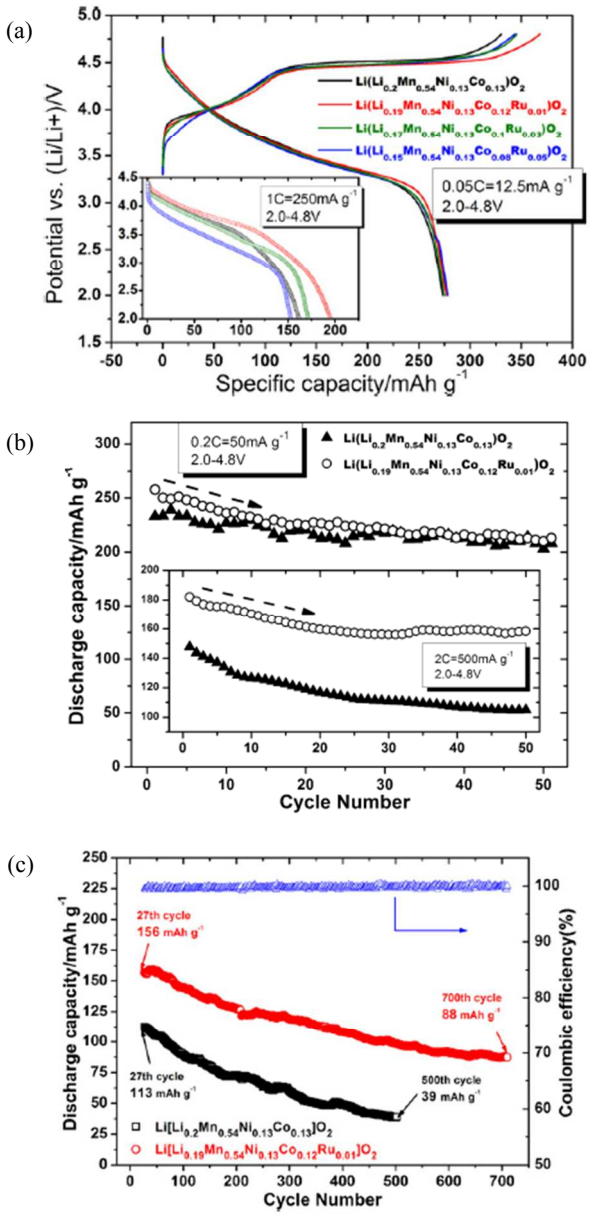

Fig. 8. (a) The 1st charge and discharge profiles vs. voltage of $Li(Li_{0.2-x}Mn_{0.54}Ni_{0.13}Co_{0.13-x}Ru_x)O_2$ (x=0, 0.01, 0.03, and 0.05) at 0.05 C rate where inset shows the performance at high rate of 1 C. (b) Cycling performance of $Li(Li_{0.2}Mn_{0.54}Ni_{0.13}Co_{0.13})O_2$ and $Li(Li_{0.19}Mn_{0.54}Ni_{0.13}Co_{0.12}Ru_{0.01})O_2$ at different rates of 0.2 C and 2 C. Testing mode of cycling for inset is 0.05 C for a first cycle followed by 2 C cycles in sequence. T=25 °C. (c) Cycling performance comparison between pristine $Li(Li_{0.2}Mn_{0.54}Ni_{0.13}Co_{0.13})O_2$ and modified $Li(Li_{0.19}Mn_{0.54}Ni_{0.13}Co_{0.12}Ru_{0.01})O_2$ as cathode materials. Testing conditions: 2 C, 2.0-4.8 V, 25 ° C [108]. Reprinted with permission from © 2012 Elsevier Ltd.

In addition to cation doping, there is some research relative to the substitution of a small amount of F^- for O^{2-} anion [106, 113]. The doped compounds, like $Li_{1+x}M_yO_{2-z}F_z$, had a smaller lattice parameter than $Li_{1+x}M_yO_2$ because the fluorine substitution changes the oxidation state of transition metal components and more Mn^{3+} ions with larger ionic radius replace Mn^{4+} ions for electro-neutrality. The content of fluorine had influence on electrochemical properties of the doped compounds. On one hand, strong Li-F bonding may hinder Li^+ extraction and lead to a low reversible capacity. On the other hand, fluorine doping makes the spinel structure more stable due to the strong M-F bonding, and this is favorable for the cyclic stability. **Figure 9a** [113] compares the discharge capacity with cycle numbers of $Li[Li_{0.2}Ni_{0.15+0.5z}Co_{0.10}Mn_{0.55-0.5z}]O_{2-z}F_z$ materials with different contents of fluorine dopant. The initial discharge capacity slightly decreased with increasing content of fluorine dopant. However, cycling performance was greatly improved, and the capacity retention after 40 cycles of the un-doped material was 79% whereas almost no capacity fade was observed in the F-doped materials. Also, cell impedance was significantly reduced by fluorine doping as shown in **Figure 9b**. When adding 10% Co to $Li[Li_{0.2}Ni_{0.2}Mn_{0.6}]O_2$, the ASI dropped significantly from 290 to 150 Ωcm^2. The fluorine doping further lowered the impedance of the material to as low as 65 Ωcm^2 for $Li(Li_{0.2}Ni_{0.175}Co_{0.1}Mn_{0.525})O_{1.95}F_{0.05}$.

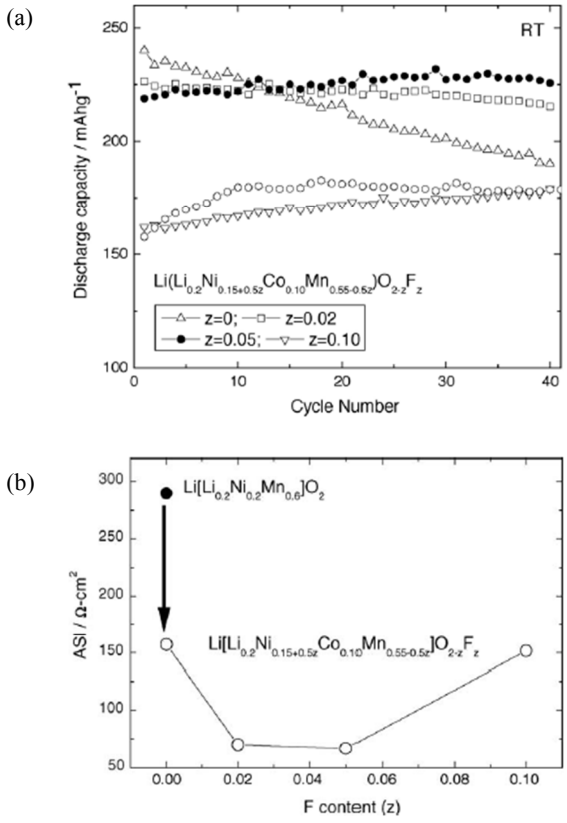

Fig. 9. (a) Discharge capacity of $Li[Li_{0.2}Ni_{0.15+0.5z}Co_{0.10}Mn_{0.55-0.5z}]O_{2-z}F_z$ cells cycled in the voltage range of 2.0-4.6 V at room temperature. Discharge capacity of $Li/Li[Li_{0.2}Ni_{0.2}Mn_{0.6}]O_2$ (open circles [o]) is also shown for comparison. (b) Average area specific impedance (ASI) at 60-80% state of charge (SOC) measured with graphite/ $Li[Li_{0.2}Ni_{0.15+0.5z}Co_{0.10}Mn_{0.55-0.5z}]O_{2-z}F_z$ cells as a function of fluorine content. (●) ASI measured with graphite/$Li[Li_{0.2}Ni_{0.2}Mn_{0.6}]O_2$ cell [113]. Reprinted with permission from © 2005 Elsevier B.V.

Composites. Physically blending two or more materials may reduce irreversible capacity and increase cathode life and rate performance [114, 115]. Blending of layered-oxides with spinel materials has been reported extensively and modeling of the improved rate capability of

batteries from blended cathodes has also been conducted [114]. Blending of LR-NMC materials with intercalation structure materials showed improved pulse power capability, cyclic capability, and capacity retention [116, 117]. For example, Gallagher et al. [116] prepared one composite cathode by blending $LiFePO_4$ with $xLi_2MnO_3 \cdot (1-x)LiMO_2$ and achieved improved performances, as shown in **Figure 10**. The capacity of the blended electrodes was ~40% higher than that without blending at a high discharge current density of 1.5 Ag^{-1}. The capacity value of the blended electrodes was a little lower than the un-blended one in low discharge current density as shown in **Figure 10a**, and the coulombic cycle efficiency was 98.1% as shown in **Figure 10b**. The improved rate capability was a result of the facile intercalation of Li-ions in the $LiFePO_4$, which showed a stable cycling performance. The stability of $LiFePO_4$ improved the cyclic property of $xLi_2MnO_3 \cdot (1-x)LiMO_2$. Owing to its low impedance, the $LiFePO_4$ carries the current demanded if the starting potential was low enough or the polarization of the electrode was large enough, which improved the pulse power capability of $xLi_2MnO_3 \cdot (1-x)LiMO_2$ (**Figure 10c**).

(a)

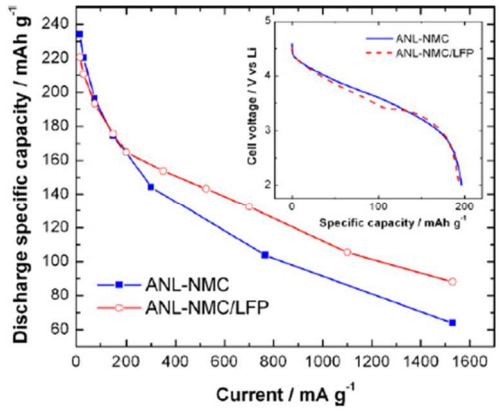

(b)

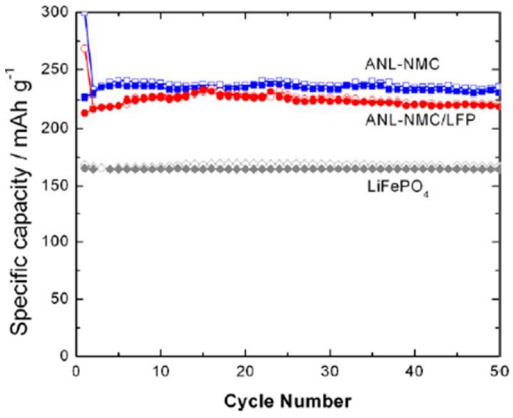

(c)

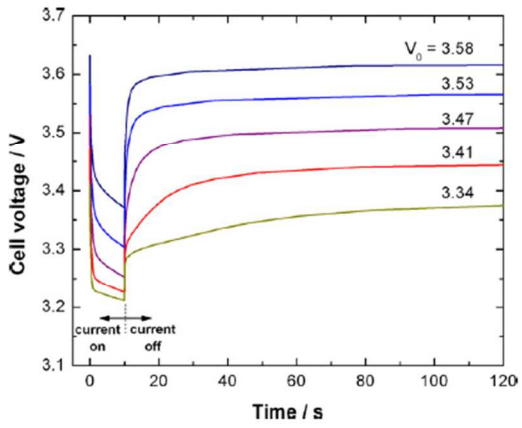

Fig. 10. (a) Rate capability for half cells of ANL-NMC and a blended active material configuration of 20 wt.% $LiFePO_4$ (LFP) and 80 wt.% ANL-NCM. (Inset) C/3 discharge rate at 75 mAg^{-1}; (b) half cell cycling results of LFP, ANL-NMC, and 80 wt.% ANL-NMC 20 wt.% LFP; (c) 3 C discharge pulses of ANL-NMC/LFP full cells from open-circuit voltages of 3.58, 3.53, 3.47, 3.41, and 3.34 V [116]. Reprinted with permission from © 2011 Elsevier B.V. Published by Elsevier B.V.

(a)

(b)

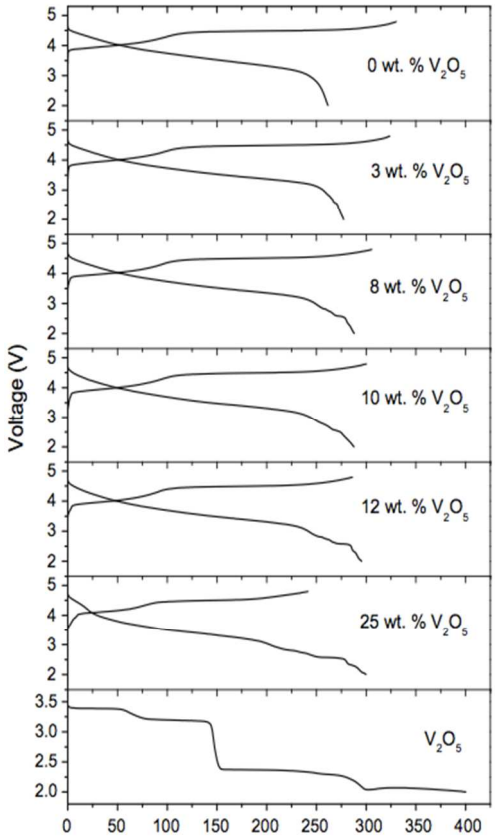

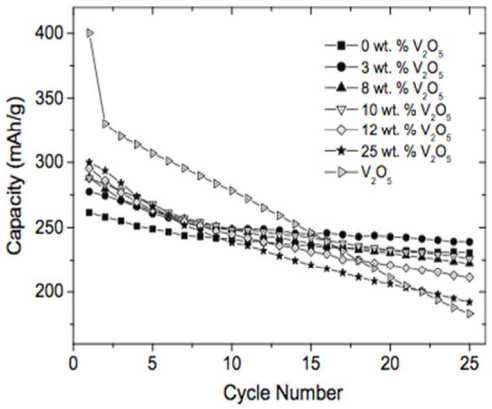

Fig. 11. (a) The first charge-discharge profiles of layered $Li[Li_{0.2}Mn_{0.54}Ni_{0.13}Co_{0.13}]O_2$, $Li[Li_{0.2}Mn_{0.54}Ni_{0.13}Co_{0.13}]O_2$-$V_2O_5$ composite with various V_2O_5 contents and V_2O_5; (b) comparison of the cycleabilities of layered $Li[Li_{0.2}Mn_{0.54}Ni_{0.13}Co_{0.13}]O_2$, V_2O_5, and $Li[Li_{0.2}Mn_{0.54}Ni_{0.13}Co_{0.13}]O_2$-$V_2O_5$ composites with various V_2O_5 contents [117]. Reprinted with permission from © 2008 Elsevier B.V.

Gao et al. [117] successfully suppressed irreversible capacity loss and increased cycle life by mixing various V_2O_5 contents with $Li[Li_{0.2}Mn_{0.54}Ni_{0.13}Co_{0.13}]O_2$. In these composites, the Li-free V_2O_5, with a capacity of about 400 $mAhg^{-1}$, served as an insertion host to accommodate the Li ions that could not be inserted back into the layered lattice after the first charge as shown in **Figures 11a**. The mechanism is: $V_2O_5 + xLi^+ + xe^- \rightarrow Li_2V_2O_5$. **Figure 11a** compares the initial voltage profiles of the $Li[Li_{0.2}Mn_{0.54}Ni_{0.13}Co_{0.13}]O_2$-$V_2O_5$ composites with those of $Li[Li_{0.2}Mn_{0.54}Ni_{0.13}Co_{0.13}]O_2$ and V_2O_5 that were recorded at 12.5 mAg^{-1}. The charge capacity decreased while the discharge capacity increased with increasing V_2O_5 content; the irreversible capacity loss in the first cycle decreased from 68 $mAhg^{-1}$ with increasing V_2O_5 content and reached zero around 11 wt.% V_2O_5. The decrease in irreversible capacity loss was due to the fact that V_2O_5 served as a host to insert back the Li ions that could not be accommodated into the layered lattice because of the elimination of some of the oxide ion vacancies and Li ion sites at the end of the first charge. The cyclic properties of this composite are shown in **Figure 11b**. The irreversible capacity loss decreased from 68 $mAhg^{-1}$ at 100% $Li[Li_{0.2}Mn_{0.54}Ni_{0.13}Co_{0.13}]O_2$ to 0 around 89 wt.% $Li[Li_{0.2}Mn_{0.54}Ni_{0.13}Co_{0.13}]O_2$-11 wt.% V_2O_5. The composite samples exhibited slightly higher capacity fade than the non-blended layered oxide samples and the capacity fade increased with increasing V_2O_5 content. The composite cathodes with about 10-12 wt.% V_2O_5 exhibited an attractive discharge capacity of close to 300 $mAhg^{-1}$ with little irreversible capacity loss and good cyclic capability.

Nanostructured materials. In general, LR-NMC materials have large particle sizes, and this may lead to poor rate capabilities. Nanostructured materials have been recently investigated in order to improve the electric performance of LR-NMC materials [30, 37]. For instance, nanostructured materials may decrease the diffusion length of Li-ion in the insertion/extraction process, which may result in high capacities at high charge-discharge rates. Nanostructured materials may also increase surface/interface storage due to the large contact interface between electrode material and electrolyte. In addition, nanostructured materials may buffer the stresses caused by volume variation occurring during charge-discharge processes, and may alleviate capacity fade and poor rate capability associated with material breaking away into electrolytes [118]. However, nanostructured materials may reduce interface stability due to their high specific surface energy. Therefore, how to build nanostructural cathode materials with high energy density and a stable interface with electrolytes is a key issue for current research on LR-NMC nanostructured materials. Recent observations in nanosized insertion materials for LIBs have led to more insight into the impact of the nanosizing. However, it remains difficult to construct a coherent picture [119-121].

In 2004, Hong et al. [37] fabricated a nanocrystalline $Li[Li_{0.2}Ni_{0.2}Mn_{0.6}]O_2$ cathode with mixed particle sizes of 80-200 nm and 1-20 um. The initial discharge capacity was about 288 $mAhg^{-1}$ when it was cycled in the voltage range of 4.8-2.0 V with a specific current of 20 mAg^{-1}. It showed 43% capacity retention when the current increased from 20 mAg^{-1} to 900 mAg^{-1}. In 2007, Kim et al. [30] prepared nanoplates like $Li_{0.93}[Li_{0.21}Co_{0.28}Mn_{0.51}]O_2$ with a size of 100 nm and a thickness of 20 nm by ion-exchange reaction. The great improvement of the $Li_{0.93}[Li_{0.21}Co_{0.28}Mn_{0.51}]O_2$ cathode was due to its nanoplate-like morphology with a thickness of 20 nm that may achieve short Li diffusion length. Later, Hong's group synthesized nanowire $Li[Ni_{0.25}Li_{0.15}Mn_{0.6}]O_2$ with a diameter of about 30 nm and obtained a first discharge capacity of 311 $mAhg^{-1}$ at 4 C [122]. Wei et al. [119] synthesized a crystal habit-tuned nanoplate $Li(Li_{0.17}Ni_{0.25}Mn_{0.58})O_2$ with a size of 5-9 nm as a cathode using the hydrothermal method. The habit-tuned nanoplate crystal structure parallels the (010) plane and is perpendicular to both [001] and [100] directions. In this structure, the proportion of (010) nanoplates was significantly increased. As shown in **Figure 12**, the initial discharge capacity was 200 $mAhg^{-1}$ under discharge potentials between 2.0-4.8 V at 6 C, and retained 80% of the capacity at 0.1 C. After 50 cycles, its capacity was 186 $mAhg^{-1}$, which showed great cyclic properties and excellent rate capability. At 6 C discharge, the crystal habit-tuned nanoplate material of $Li(Li_{0.17}Ni_{0.25}Mn_{0.58})O_2$ (HTN-LNMO) has a capacity of 186 $mAhg^{-1}$ in comparison with 106 $mAhg^{-1}$ for the conventional thermodynamic equiLIBsrium nanoplate material of $Li(Li_{0.15}Ni_{0.25}Mn_{0.6})O_2$ (CN-LNMO) and 40 $mAhg^{-1}$ for $Li(Li_{0.17}Ni_{0.25}Mn_{0.58})O_2$ (LNMO) big particles. It was obvious that the excellent rate-capability of HTN-LNMO originated from the nanometer-size effect and its unique crystal structure.

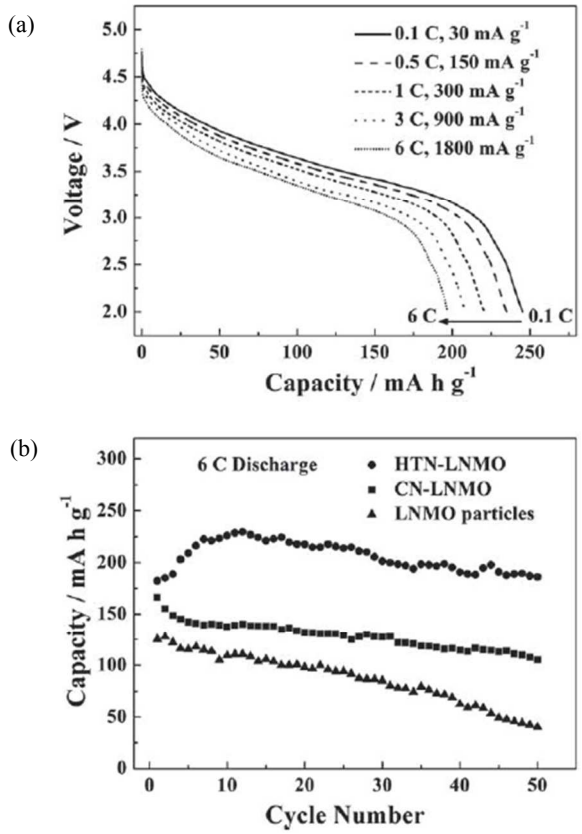

Fig. 12. Cycleability and rate capability of HTN-LNMO. a) Stabilized discharge voltage profiles of HTN-LNMO cycled at different rates: 6, 3, 1, 0.5, and 0.1 C from bottom to top. b) Discharge capacity at a 6 C rate and cycleability of HTN-LNMO compared with CN-LNMO and LNMO particles [119]. Reprinted with permission from © 2010 WILEY-VCH Verlag GmbH & Co. KGaA, Weinheim.

It seems that nanostructured materials, especially single-phase nanostructured materials, may not be an ideal solution to meet the requirements of cathodes for power LIBs. One of the primary reasons is that some of the intrinsic material properties of bulk phase, such as low conductivities, low energy densities at high charge-discharge rates, and weak mechanical stabilities, cannot be simply altered or improved by just transforming them into nanostructured materials. Without surface protection, nanostructured materials may also have more safety concerns due to their high surface reactivity, and may aggravate capacity fade due to aggregation [123, 124].

Other methods. One new method involves the development of heterogeneous nanostructured materials that are composed of multi-nanocomponents, each of which is tailored to address a specific demand (high Li-ion/electric conductivity, high capacity and structural stability). Potential synergistic effects may be achieved by the interplay between particle shape, properties, and possible association of the individual components, which can be regulated to explore the full potential of the materials in terms of performance [125, 126]. For instances, the construction of composition gradient from surface to bulk to form core-shell structured particles; a high-capacity Li- and Co-rich cathode material $Li_{1.15}[Ni_{1/3}Co_{1/3}Mn_{1/3}]_{0.85}O_2$ can be used as the core and a Li-rich and Co-free composition $Li_{1.15}[Ni_{1/4}Mn_{3/4}]_{0.85}O_2$ can be used as the shell [126] as shown in **Figure 13a**. By introducing composition gradient, the performance of core active materials can be maintained, while the less active shell materials can act as a buffer layer and help to improve the material performance at the surface. A synergistic effect of the two materials was reported by the formation of the core-shell architecture. Of note, the core-shell structured cathode material presented improved Li intercalation stability compared to the core, and improved rate capability compared to the shell as shown in **Figures 13b** and **13c**. The core-shell cathode had a smaller capacity than that of the shell cathode, but a bigger capacity than that of the core cathode (**Figure 13b**). The resistance of the core-shell cell was much smaller than that of the shell cell because of Co, which resulted in improved electric conductivity (**Figure 13c**). This result showed that the construction of the core-shell architecture, using Co-containing compounds as the core, was effective at improving rate capability.

Another new approach to improve performance of LR-NMC materials is called pre-cycling treatment [127-129]. In 2010, Ito et al. [129] studied Li-rich layered cathode $Li[Ni_{0.17}Li_{0.2}Co_{0.07}Mn_{0.56}]O_2$ material with and without pre-cycling treatment; the pre-cycling treatment included increasing the upper potential limit by 0.1 V every two cycles from 4.5 V to 4.8 V. Results showed that the pre-cycling treatment effectively depressed the formation of micro-cracks on the surface of the crystals and the lattice distortion in the crystals. Similarly, in 2012, Nakahara et al. [127] fabricated a Fe-containing Li-rich layered oxide $Li_{1.26}Mn_{0.52}Fe_{0.22}O_2$ and evaluated graphite/$Li_{1.26}Mn_{0.52}Fe_{0.22}O_2$ cells after a stepwise pre-cycling treatment. The pre-cycling treatment drastically increased the specific capacity of the $Li_{1.26}Mn_{0.52}Fe_{0.22}O_2$ from 167 to 236 $mAhg^{-1}$. Other properties such as operation voltage, discharge rate capability, and cycleability also improved with this treatment.

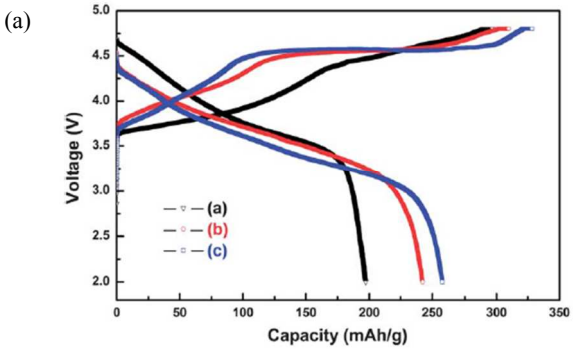

(b)

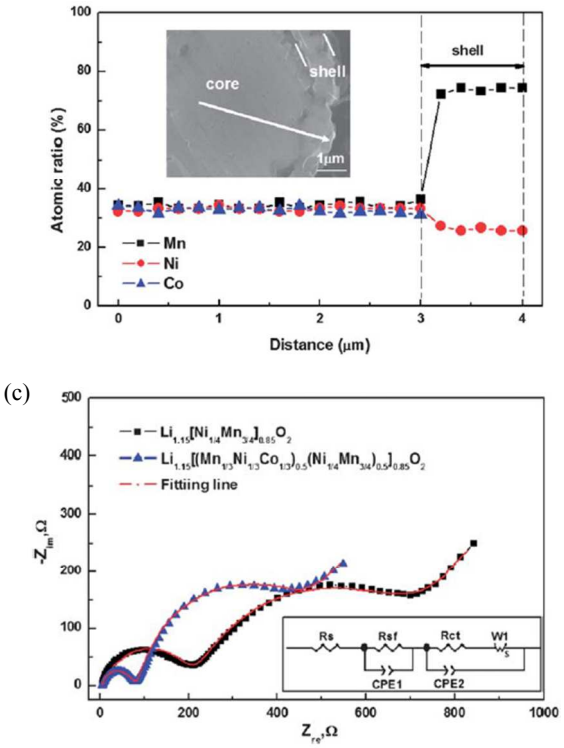

Fig. 13. (a) Electron probe microanalyzer (EPMA) compositional change from the cross-section of the core-shell structured $Li_{1.15}[(Mn_{1/3}Ni_{1/3}Co_{1/3})_{0.5}(Ni_{1/4}Mn_{3/4})_{0.5}]_{0.85}O_2$ particle. (b) The initial charge-discharge curves of [a] $Li_{1.15}[Ni_{1/3}Co_{1/3}Mn_{1/3}]_{0.85}O_2$, [b] core-shell structured $Li_{1.15}[(Mn_{1/3}Ni_{1/3}Co_{1/3})_{0.5}(Ni_{1/4}Mn_{3/4})_{0.5}]_{0.85}O_2$ and [c] $Li_{1.15}[Ni_{1/4}Mn_{3/4}]_{0.85}O_2$ in the voltage range of 2.0-4.8 V at a rate of 0.1 C. (c) Impedance spectra of Li/ $Li_{1.15}[(Mn_{1/3}Ni_{1/3}Co_{1/3})_{0.5}(Ni_{1/4}Mn_{3/4})_{0.5}]_{0.85}O_2$ cells and Li/ $Li_{1.15}[Ni_{1/4}Mn_{3/4}]_{0.85}O_2$ cells [126]. Reprinted with permission from © 2012, Royal Society of Chemistry.

Conclusions and outlook

In this review, the problems with Li-rich layered LR-NMC materials have been reviewed. Some key questions of LR-NMC need to be addressed for this family of materials before their widely application: voltage fade and hysteresis represent significant challenges to the commercialization of these oxides. Mitigating voltage fade will enable the use of these high-energy materials for PHEV and EV applications. In addition, the charge-discharge mechanism of such materials is still not clear. Moreover, the problems of large initial irreversible capacity loss and inferior rate and cyclic capabilities still exist and need to be further studied. Lastly, these materials have low tap density and it is difficult to obtain dense materials. Therefore, researchers need to find ways to increase energy density and, at the same time, reduce production cost.

However, the conventional strategies discussed in this paper have limited effects for improving the whole performance of such materials. For example, the mechanisms of voltage fade and hysteresis are still not clear and there are no effective ways to control them. The following ideas, which may lead to better understanding and improvements of LMR-NMC, may be considered:

(1) Solve structural and electrochemical performance problems from structural designing and electrochemical characterization. For instance, develop an atomic-level model to capture the essential electrochemical observations associated with voltage fade and hysteresis to understand the following questions: (a) what are the effects of domains and domain size? (b) How does the transition metal and Li ordering influence the electrochemical performance? (c) How can the transition metal and Li return to the octahedral positions in LMR-NMC? (d) How do the transition metal and Li migrate to a new octahedral position? (e) How can the transition metal and Li be trapped in the octahedral positions thereby increasing cell impedance? (f) Does the H^+ inserts into the lattice of structure during discharge?

(2) Understand oxygen loss mechanism and corresponding formation of defect sites. For example, develop a kind of redox shuttle electrolyte additives to stabilize SEI and to capture the intermediate oxygen anions released from LR-NMC lattice during discharge. Oxygen release is one of the biggest safety issues because of the high voltage applied. Overcharge of LR-NMC based batteries can lead to side reactions, rapid temperature elevation, and even explosion. On the overcharged cathode surface, the redox shuttle molecule is oxidized to its cation form which, via diffusion across the electrolyte, would be reduced back to its original or reduced state on the surface of the anode. The reduced form would then diffuse back to the cathode and oxidize again. The "oxidation-diffusion-reduction-diffusion" cycle can be repeated continuously due to the reversible nature of the redox shuttle to shunt the overcharge current. On the other hand, these additives should capture the intermediate oxygen anions or radicals before forming oxygen.

(3) Form unique nano-layered porous cathodes using electrostatic layer-by-layer self-assembly to enhance energy/power densities and pulse power densities. Nano-layered cathodes can be fabricated on aluminum current collectors by alternate adsorption of oppositely charged active materials and highly conductive additive materials. Based on our previous studies [130-134], we expect electrostatic layer-by-layer self-assembly allow tuning of the interface properties between cathode active particles and additive polymers, and cathode active particles and electrolyte. Their porous structure may act as reservoirs for liquid electrolytes capable of fast Li-ion conduction, and their highly intertwined component materials may facilitate electric conductivity and Li-ion transport. Such nano-layered structures may also provide large reactive interfacial areas that allow convenient incorporation and manipulation of active materials into specific nano-layers. The nano-layer/electrolyte interfaces can be tuned to enhance electronic and ionic conduction across the interfaces therefore leading to maximized efficiency of active materials. What's more, the energy density may be improved without binder and the pulse power may be improved by tuning the thickness of cathode nano-layers.

Acknowledgement

The authors wish to acknowledge the financial support of the West Virginia Higher Education Policy Commission Division of Science Research Challenge Grant program. The authors thank Suzanne Danley for proofreading.

References

[1] J. B. Goodenough and K. S Park, *J. Am. Chem. Soc.*, 2013, **135**, 1167
[2] M. Armand and J.M. Tarascon, *Nature*, 2008, **451**, 652
[3] S. Akao, M. Yamada, T. Kodera, K. Myoujin, and T. Ogihara, *Advances in Materials Science and Engineering*, 2011, **2011**, 1
[4] J. B. Goodenough and Y. Kim, *Chem. Mater.*, 2010, **22**, 587
[5] M. S Whittingham, *Chem. Rev.*, 2004, **104**, 4271
[6] T. Watabe and M. Mori, *LIBs materials industry*, 2011, **26 January**, 22
[7] http://www.greencarcongress.com/2012/02/envia-20120227.html , 2013
[8] Working Document of the NPC Future Transportation Fuels Study, 2012,
[9] M. M. Thackeray, C. S. Johnson, J. T. Vaughey, N. Li and S. A. Hackne, *J. Mater. Chem.*, 2005, **15**, 2257
[10] M. N. Ates, Q. Jia, A. Shah, A. Busnaina, S. Mukerjee and K. M. Abraham. *J. Electrochem. Soc.*, 2014, **161**, A290
[11] C. S. Johnson, N. Li, C. Lefief, J. T. Vaughey, and M. M. Thackeray, *Chem. Mater.*, 2008, **20**, 6095
[12] K. Jarvis, Z. Deng, L. Allard, A. Manthiram and P. Ferreira. *Microscopy and Microanalysis*, 2011, **17**, 1578
[13] C. S. Johnson, S. D. Korte, J. T. Vaughey, et al., *J. Power Sources*, 1999, **81-82**, 491
[14] A. Boulineau, L. Croguennec, C. Delmas, and F. Weill, *Chem. Mater.,* 2009, **21**, 4216
[15] G. Yang, H. Ji, P. Gao, A. Hong, H. Ding, S. Roy, J. Pinto and X. Jiang, *J. Electrochem. Soc.,* 2011, **158**, A1071
[16] J. Jiang and J.R. Dahn, *Electrochim Acta,* 2005, **50**, 4778
[17] J. Jiang and J.R. Dahn, *Electrochim Acta,* 2006, **51**, 3413
[18] Z. H. Lu, D. D. MacNeil, J. R. Dahn, *Electrochem Solid ST*, 2001, **4**, A191
[19] Z. H. Lu, L. Y. Beaulieu, R. A. Donaberger, C. L. Thomas, J. R. Dahn, *J. Electrochem. Soc.*, 2002, **149**, A778
[20] R. Santhanam, P. Jones, A. Sumana, B. Rambabu, *J. Power Sources*, 2010, **195**, 7391
[21] S.-H. Kang, J. Kim, D. Abraham, M. E. Stoll, Y.-K. Sun, K. Amine, *J. Power Sources*, 2002, **112**, 41
[22] K-S. Park, M. H. Cho, S. J. Jin, C. H. Song, K. S. Nahm, *J. Power Sources*, 2005, **146**, 281
[23] M. Tabuchi, Y. Nabeshima, K. Ado, M. Shikano, H. Kageyama, K. Tatsumi, *J. Power Sources*, 2007, **174**, 554
[24] C. Pan, Y. J. Lee, B. Ammundsen, and C. P. Grey, *Chem. Mater.,* 2002, **14**, 2289
[25] Z. H. Lu, Z. H. Chen, and J. R. Dahn, *Chem. Mater.,* 2003, **15**, 3214
[26] C.H. Lei, J. Bareno, J.G. Wen, I. Petrov, S.-H. Kang, D.P. Abraham, *J. Power Sources,* 2008, **178**, 422
[27] K. A. Jarvis, Z. Deng, L. F. Allard, Arumugam Manthiram, and Paulo J. Ferreira, *Chem. Mater.,* 2011, **23**, 3614
[28] J-S. Kim, C. S. Johnson, J. T. Vaughey, and M. M. Thackeray, *Chem. Mater.,* 2004, **16**, 1996
[29] J. Bareno, M. Balasubramanian, S.H. Kang, J.G. Wen, C.H. Lei, S.V. Pol, I. Petrov and D.P. Abraham. *Chem. Mater.,* 2011, **23**, 2039
[30] Y-J Kim, Y. Hong, M. G Kim and J. Cho, *Electrochem Commun*, 2007, **9**, 1041
[31] H. Yu, H. Kim, Y. Wang, P. He, Daisuke Asakura, Yumiko Nakamura and Haoshen Zhou, *Phys. Chem. Chem. Phys*., 2012, **14**, 6584
[32] X. Yu, Y. Lyu, L. Gu, H. Wu, S. Bak, Y. Zhou, K. Amine, S. N. Ehrlich, H. Li, K. Nam and X.Yang, *Adv. Energy Mater*., 2014, **4**, 1300950
[33] S-H Yu, T. Yoon, J. Mun, S. Park, Y-S Kang, J-H Park, Seung M. Oh and Yung-Eun Sung, *J. Mater. Chem. A*, 2013, **1**, 2833
[34] D. Mohanty, S. Kalnaus, R. A. Meisner, K. J. Rhodes, J. Li, E. A. Payzant, D. L. Wood, C. Daniel, *J. Power Sources*, 2013, **229**, 239
[35] B. Song, Z. Liu, M. Lai and L. Lu, *Phys. Chem. Chem. Phys.*, 2012, **14**, 12875
[36] N. Yabuuchi, K. Yoshii, S-T. Myung, I. Nakai, and S. Komaba, *J. Am. Chem. Soc.*, 2011, **133**, 4404
[37] Y-S Hong, Y. J. Park, K. S. Ryu, S. H. Chang and M. G. Kim, *J. Mater. Chem.*, 2004, **14**, 1424
[38] Y. Wu and A. Manthiram, *Electrochem Solid ST*, 2007, **10**, A151
[39] Y. Koyamaa, I. Tanakaa, M. Nagao, R. Kanno, *J. Power Sources*, 2009, **189**, 798
[40] L. Yu, W. Qiu, F. Lian, J. Huang, X. Kang, *J. Alloy Compd*, 2009, **471**, 317
[41] M. Gu, I. Belharouak, J. Zheng, H. Wu, J. Xiao, A. Genc, K. Amine, S. Thevuthasan, D.R. Baer, J. Zhang, N.D. Browning, J. Liu and C. Wang, *ACS Nano*, 2013, **7**, 760
[42] A.R. Armstrong, M. Holzapfel, P. Novák, C.S. Johnson, S.H. Kang, M.M. Thackeray, P.G. Bruce, *J. Am. Chem. Soc.,* 2006, **128**, 8694
[43] P. Xiao, Z. Q. Deng, A. Manthiram, and G. Henkelman, *J. Phys. Chem. C*, 2012, **116**, 23201
[44] T. A. Arunkumar, Y. Wu, and A. Manthiram, *Chem. Mater.,* 2007, **19**, 3067
[45] A. D. Robertson and P. G. Bruce, *Chem. Commun*., 2002, **2002**, 2790
[46] A. R. Armstrong, A.D. Robertson, P.G. Bruce, *J. Power Sources*, 2005, **146**, 2275
[47] C. S. Johnson, N. Li, C. Lefief, M. M. Thackeray, *Electrochem Commun*, 2007, **9**, 787
[48] B. Li, Q. Wang, Y. Zhang, Z. Song, D. Yang, Int. *J. Electrochem. Sci.,* 2013, **8**, 5396
[49] M. M. Thackeray, S-H Kang, C. S. Johnson, J. T. Vaughey, R. Benedeka and S. A. Hackney, *J. Mater. Chem.*, 2007, **17**, 3112
[50] C. Yu, G. Li, X. Guan, J. Zheng, D. Luo and L. Li, *Phys. Chem. Chem. Phys.*, 2012, **14**, 12368
[51] A.D. Robertson, P.G. Bruce, *Electrochem Solid ST*, 2004, **7**, A294
[52] S.E. Trask,Y. Li, J.J. Kubai, M. Bettge, B.J. Polzin, Y. Zhu, A.N. Jansen, D.P. Abraham, *J. Power Sources*, 2014, **259**, 233
[53] K.G. Gallagher, J.R. Croy, M. Balasubramanian, M. Bettge, D.P. Abraham, A.K. Burrell and M.M. Thackeray. *Electrochem Commun*, 2013, **33**, 96
[54] M. Bettge, Y. Li, K.G. Gallagher, Y. Zhu, Q. Wu, W. Lu, I. Bloom and D.P. Abraham. *J. Electrocheml Sci*., 2013, **160**, A2046
[55] I. Bloom, L. Trahey, A. Abouimrane, I. Belharouak, H. Wu, W. Lu, D.P. Abraham, M. Bettge, J. Elam, X. Meng and A. Burrell. *J. Power Source,* 2013, **249**, 509
[56] J.R. Croy et al., *J. Electrochem Sci.*, 2014, **161**, A318
[57] Y.-S. Hong, Y.J. Park, X. Wu, K.S. Ryu, S.H. Chang, *Solid-State Lett.,* 2003, **6**, A166
[58] S.-H. Kang, Y.-K. Sun, K. Amine, *Electrochem. Solid ST*, 2003, **6**, A183
[59] Y. Liu and S. Liu, *Ionics*, 2013, **19**, 477
[60] S. H. Kang and K. Amine, *J. Power Sources*, 2003, **124**, 533
[61] K. Ozawa, Y. Nakao, T. Mochiku, Z. Cheng, L. Wang, H. Iwai, Y. Tsuchiya, H. Fujii and N. Igawa, *J. Electrochem. Soc*., 2012, **159**, A300

[62] J. Li, R. Klöpsch, M.C. Stan, S. Nowak, M. Kunze, M. Winter, S. Passerini, *J. Power Sources,* 2011, **196**, 4821
[63] Y.N. Ko, J-H Kim, J-K Lee, Y.C. Kanga, J-H Lee, *Electrochim Acta*, 2012, **69**, 345
[64] Y-J Hong, J-H Kim, M-H Kim, Y-C Kang, *Materials Research Bulletin*, 2012, **47**, 2022
[65] X. Zhang, C. Yu, X. Huang, J. Zheng, X. Guan, D. Luo, L. Li, *Electrochim Acta*, 2012, **81**, 233
[66] S.J. Shi, J.P. Tu, Y.Y. Tang, Y.X. Yu, Y.Q. Zhang, X.L. Wang, C.D. Gu, *J. Power Sources*, 2013, **228**, 14
[67] C. Yu, G. Li, X. Guan, J. Zheng, L. Li, T. Chen, *Electrochim Acta*, 2012, **81**, 283
[68] Z. Li, K. Zhu, Y.H. Wang, C.Z. Wang, G. Chen, Y.J. Wei, *Science of Advanced Materials,* 2012, **4**, 843
[69] R. Santhanam, B. Rambabu, Int. *J. Electrochem. Sci.,* 2009, **4**, 1770
[70] X. Huang, Q. Zhang, H. Chang, J. Gan, H. Yue and Y. Yang, *J. Electrochem. Soc.*, 2009, **156**, A162
[71] M. Tabuchi, Y. Nabeshimaa, T. Takeuchia, H. Kageyamaa, K. Tatsumia, J. Akimotob, H. Shibuyac, J. Imaizumi, *J. Power Sources*, 2011, **196**, 3611
[72] W.C. West, J. Soler, B.V. Ratnakumar, J. Power Sources, 2012, 204, 200
[73] M. Tabuchi, Y. Nabeshima, T. Takeuchi, H. Kageyama, J. Imaizumi, H. Shibuya, J. Akimoto, *J. Power Sources*, 2013, **221**, 427
[74] J.R. Croy, S.H. Kang, M. Balasubramanian, M.M. Thackeray, *Electrochem Commun*, 2011, **13**, 1063
[75] J. Lin, D. Mu, Y. Jin, B. Wu, Y. Ma, F. Wu, J. *Power Sources*, 2013, **230**, 76
[76] F. Wu, H. Lu, Y. Su, N. Li. L, Bao. S, Chen, *J. Appl Electrochem*, 2010, **40**, 783
[77] Z. Chen, Y. Qin, Khalil Amine and Y.-K. Sun, *J. Mater. Chem.,* 2010, **20**, 7606
[78] J-H. Ryu, B-G Park, S-B Kim, Y-J Park, *J. Appl Electrochem*, 2009, **39**, 1059
[79] Y. Wu, A. Manthiram, *Solid State Ionics*, 2009, **180**, 50
[80] Y. Deng, S. Liu, X. Liang, *J. Solid State Electrochem*, 2013, **17**, 1067
[81] Myung S T, Izumi K, Komaba S, et al. *J. Phys. Chem. C*, 2007, **111**, 4061
[82] J. M. Zheng, J. Li, Z.R. Zhang, X.J. Guo, Y. Yang. *Solid State Ionics*. 2008, **179**, 1794
[83] Y. Wu and A. Manthiram, *Electrochem Solid ST*, 2006, **9**, A221
[84] S.J. Shi, J.P. Tu, Y.Y. Tang, X.Y. Liu, Y.Q. Zhang, X.L. Wang, C.D. Gu, *Electrochim Acta*, 2013, **88**, 671
[85] Y. Zhao, C. Zhao, H. Feng, Z. Sun and D. Xia, *Solid-State Lett.,* 2011, **14**, A1
[86] X. Guan, B. Ding, X. Liu, J. Zhu, C. Mi, X. Zhang, *J. Solid State Electrochem,* 2013, **17**, 2087
[87] K-J. Rosina, M. Jiang, D. Zeng, E. Salager, A-S. Best and C-P. Grey, *J. Mater. Chem.*, 2012, **22**, 20602
[88] G.R. Li, X. Feng, Y. Ding, S.H. Ye, X.P. Gao, *Electrochim Acta,* 2012, **78**, 308
[89] K. Yang, L. Fan, J. Guo, X. Qu, *Electrochim Acta*, 2012, **63**, 363
[90] H. Deng, I. Belharouak, C.S. Yoon, Y.K. Sun, K. Amine, *J. Electrochem. Soc.*, 2010, **157**, A1035
[91] S-H Lee, B-K Koo, J-C Kim, K-M Kim, *J. Power Sources*, 2008, **184**, 276
[92] Wang Q Y, Liu J, Murugan A V, et al. *J. Mater. Chem.,* 2009, **19**, 4965
[93] B. Liu, Q. Zhang, S. He, Y. Sato, J. Zheng, D. Li, *Electrochim Acta*, 2011, **56**, 6748
[94] S.H. Kang, M.M. Thackeray, *Electrochem Commun*, 2009, **11**, 748
[95] Q. Q. Qiao, H. Z. Zhang, G. R. Li, S. H. Ye, C. W. Wang and X. P. Gao, *J. Mater. Chem. A*, 2013, **1**, 5262
[96] Y.J. Kang, J.H. Kim, S.W. Lee, et al., *Electrochim Acta.,* 2005, **50**, 4784
[97] S. Myung, K. Amine, Y. Sun, *J. Mater. Chem.*, 2010, **20**, 7074
[98] J.S. Kim, C.S. Johnson, J.T. Vaughey and M.M. Thackeray, *J. Power Sources*, 2006, **153**, 258
[99] Y.W.Y. Denis, Y. Katsunori, N. Hiroshi, *J. Electrochem Soc*, 2010, **157**, A1177
[100] A. Abouimrane, O.C. Compton, H. Deng, et al., *Electrochem Solid ST*, 2011, **14**, A126
[101] H. Z. Zhang, Q. Q. Qiao, G. R. Li, S. H. Ye and X. P. Gao, *J. Mater. Chem.,* 2012, **22**, 13104
[102] J. Zheng, S. Deng, Z. Shi, H. Xu, H. Xu, Y. Deng, Z. Zhang, G. Chen, *J. Power Sources,* 2013, **221**, 108
[103] M. Chi, C. Fell, Bo Xu, and S. Meng, *Microsc. Microanal*, 2011, **17**, 1574
[104] Z. Tang, Z. Wang, X. Li, W. Peng, *J. Power Sources*, 2012, **204**, 187
[105] J.H. Kim, C.W. Park, Y.K. Sun, *Solid State Ionics*, 2003, **164**, 43
[106] O. Sha, Z. Tang, S. Wang, W. Yuan, Z. Qiao, Q. Xu, L. Ma, *Electrochim Acta*, 2012, **77**, 250
[107] S.H. Park, Y.K. Sun, *J. Power Sources*, 2003, **119-121**, 161
[108] B. Song, M. Lai, L. Lu, *Electrochim Acta*., 2012, **80**, 187
[109] L. Jiao, M. Zhang, H. Yuan, M. Zhao, J. Guo, W. Wang, X. Zhou, Y. Wang, *J. Power Sources*, 2007, **167**, 178
[110] Q. Liu, K. Du, G. Hu, Z. Peng, Y. Cao, W. Liu, *Solid State Ionics*, 2012, **227**, 23
[111] A. Boulineau, L. Simonin, J. Colin, E. Canévet, L. Daniel, and S. Patoux, *Chem. Mater.*, 2012, **24**, 3558
[112] M-K Song, S Park, F.M. Alamgir, J. Cho, M. Liu, *Materials Science and Engineering R*, 2011, **72**, 203
[113] S.H. Kang, K.J. Amine, *J. Power Sources*, 2005, **146**, 654-656
[114] P.M. Gomadam, D.R. Merritt, E.R. Scott, C.L. Schmidt, P.M. Skarstad, J.W. Weidner, *J. Power Sources*, 2007, **174**, 872
[115] A. Manthiram and W. Choi, *Electrochem and Solid ST*, 2007, **1**0, A228
[116] K. G. Gallagher, S-H Kang, S. Park, S-Y Han, *J. Power Sources*, 2011, **19**6, 9702
[117] J. Gao, J. Kim, A. Manthiram, *Electrochem Commun*, 2009, **11**, 84
[118] R. Liu, J. Duay and S. Lee, *Chemical Communications*, 2010, **47**, 1384
[119] G. Wei, X. Lu, F. Ke, L. Huang, J. Li, Z. Wang, Z. Zhou, and S. Sun, *Adv. Mater.,* 2010, **22**, 4364
[120] Y.J. Wei, K. Nikolowski, S.Y. Zhan, H. Ehrenberg, S. Oswald, G. Chen, C.Z. Wang, H. Chen, *Electrochem Commun*, 2009, **11**, 2008
[121] C. Zhao, W. Kang, Q. Xue, Q. Shen, *J. Nanopart Res*, 2012, **14**, 1240
[122] M.G. Kim, M. Jo, Y.S. Hong, et al. *Chem. Commun.,* 2009, **2**, 218
[123] R. Liu, J. Duay & S. Lee, *Chem. Commun.,* 2011, **47**, 1384
[124] Y. Sun, S. Myung, B. Park, J. Prakash, I. Belharouak & K. Amine, *Nature Mater.,* 2009, **8**, 320
[125] Z. Chen, D-J Lee, Y-K Sun, and K. Amine, *MRS Bulletin*, 2011, **36**, 498
[126] X. Yang, X. Wang, Q. Wei, H. Shu, L. Liu, S. Yang, B. Hu, Y. Song, G. Zou, L. Hu and L. Yi. *J. Mater. Chem.,* 2012, **22**, 19666
[127] K. Nakahara, M. Tabuchi, S. Kuroshima, A. Toda, K. Tanimoto, and K. Nakano, *J. Electrochem. Soc.,* 2012, **159**, A1398

[128] A. Watanabe, F. Matsumoto, M. Fukunishi, G. Kobayashi, A. Ito, M. Hatano, Y. Ohsawa and Y. Sato, J. *Electrochem. Sci.*, 2011, **80**, 561
[129] A. Ito, D. Li, Y. Sato, M. Arao, M. Watanabe, M. Hatano, H. Horie, Y. Ohsawa, *J. Power Sources*, 2010, **195**, 567
[130] B. Li, B. Jiang, D.J. Fauth, M.L. Gray, H.W. Pennline, G.A. Richards. *Chem. Comm.,* 2011, **47**, 1719
[131] B. Jiang, V. Kish, D.J. Fauth, M.L. Gray, H.W. Pennline, B. Li, Int. *J. Greenh Gas Con*, 2011, **5**, 1170
[132] Q. Zhao, H. Li, B. Li, *J. Mater Res*, 2011, **26**, 347
[133] Q. Zhao, B. Li, *Nanomed-Nanotechnol*, 2008, **4**, 302
[134] F. Likibi, B. Jiang, B. Li, *J. Mater Res*, 2008, **23**, 3222